SIAM J. SCI. COMPUT.
Vol. 40, No. 2, pp. A1034–A1062

RANGE-SEPARATED TENSOR FORMAT FOR MANY-PARTICLE MODELING*

PETER BENNER†, VENERA KHOROMSKAIA‡, AND BORIS N. KHOROMSKIJ§

Abstract. We introduce and analyze the new range-separated (RS) canonical/Tucker tensor format which aims for numerical modeling of the 3D long-range interaction potentials in multiparticle systems. The main idea of the RS tensor format is the independent grid-based low-rank representation of the localized and global parts in the target tensor, which allows the efficient numerical approximation of N-particle interaction potentials. The single-particle reference potential, described by the radial basis function $p(\|x\|)$, $x \in \mathbb{R}^d$, say $p(\|x\|) = 1/\|x\|$ for $d = 3$, is split into a sum of localized and long-range low-rank canonical tensors represented on a fine 3D $n \times n \times n$ Cartesian grid. The smoothed long-range contribution to the total potential sum is represented on the 3D grid in $O(n)$ storage via the low-rank canonical/Tucker tensor. We prove that the Tucker rank parameters depend only logarithmically on the number of particles N and the grid size n. Agglomeration of the short-range part in the sum is reduced to an independent treatment of N localized terms with almost disjoint effective supports, calculated in $O(N)$ operations. Thus, the cumulated sum of short-range clusters is parametrized by a single low-rank canonical reference tensor with local support, accomplished by a list of particle coordinates and their charges. The RS canonical/Tucker tensor representations defined on the fine $n \times n \times n$ Cartesian grid reduce the cost of multilinear algebraic operations on the 3D potential sums, arising in modeling of the multidimensional data by radial basis functions. For instance, computation of the electrostatic potential of a large biomolecule and the interaction energy of a many-particle system, 3D integration and convolution transforms as well as low-parametric fitting of multidimensional scattered data all are reduced to 1D calculations.

Key words. low-rank tensors, summation of electrostatic potentials, long-range many-particle interactions, radial basis functions, canonical and Tucker tensor formats, Ewald summation

AMS subject classifications. 65F30, 65F50, 65N35, 65F10

DOI. 10.1137/16M1098930

1. Introduction.

Numerical treatment of long-range potentials is a challenging task in the computer modeling of multiparticle systems, for example, in molecular dynamic simulations of large solvated biological systems such as proteins, in the analysis of periodic Coulombic systems or scattered data in geosciences, and in Monte Carlo sampling, and so on [50, 19, 30, 53, 46, 23]. For a given nonlocal generating kernel $p(\|x\|)$, $x \in \mathbb{R}^3$, the calculation of a weighted sum of interaction potentials in the large N-particle system, with the particle locations at $x_\nu \in \mathbb{R}^3$, $\nu = 1, \dots, N$,

$$P(x) = \sum\nolimits_{\nu=1}^{N} z_\nu \, p(\|x - x_\nu\|), \quad z_\nu \in \mathbb{R}, \quad x_\nu, x \in \Omega = [-b, b]^3, \tag{1.1}$$

leads to a computationally intensive numerical task. Indeed, the generating radial basis function $p(\|x\|)$ is allowed to have a slow polynomial decay in $1/\|x\|$ as $\|x\| \to \infty$ so that each individual term in (1.1) contributes essentially to the total potential at

*Submitted to the journal's Methods and Algorithms for Scientific Computing section October 14, 2016; accepted for publication (in revised form) October 18, 2017; published electronically April 5, 2018.

http://www.siam.org/journals/sisc/40-2/M109893.html

†Max-Planck Institute for Dynamics of Complex Technical Systems, D-39106 Magdeburg, Germany (benner@mpi-magdeburg.mpg.de).

‡Max-Planck-Institute for Mathematics in the Sciences, D-04103 Leipzig, Germany (vekh@mis.mpg.de), and Max-Planck Institute for Dynamics of Complex Technical Systems, D-39106 Magdeburg, Germany.

§Max-Planck-Institute for Mathematics in the Sciences, D-04103 Leipzig, Germany (bokh@mis.mpg.de).

each point in the computational domain Ω, thus predicting the $O(N)$ complexity for the straightforward summation at every fixed target $x \in \mathbb{R}^3$. Moreover, in general, the function $p(\|x\|)$ has a singularity or a cusp at the origin, $x = 0$, making its full-grid representation problematic. Typical examples of the radial basis functions $p(\|x\|)$ are given by the Newton $1/\|x\|$, Slater $e^{-\lambda\|x\|}$, Yukawa/Helmholtz $e^{-\lambda\|x\|}/\|x\|$, and other Green's kernels (see examples in section 4.1).

The traditional approaches based on the Ewald summation method [22] combined with the fast Fourier transform (FFT) usually apply to calculations of the interaction energy or the interparticle forces of a system of N particles with periodic closure, which reduces the complexity scaling in the particle number from $O(N^2)$ to $O(N \log N)$ [19, 20]. These approaches need meshing up the result of Ewald sums over a 3D Cartesian grid for the charge assignment onto an $n_m \times n_m \times n_m$ mesh. Generation of the smoothed charge distribution on the right-hand side of the arising Poisson equation is the main complexity limitation, since it requires N-term summation of the grid functions of size $O(n_m^3)$, presuming the dominating cost $O(n_m^3 N)$. This procedure is accomplished by the cheap FFT solver with periodic boundary conditions that amounts to $O(n_m^3 \log n_m)$ operations. The mesh implementation approaches trace back to the original so-called particle-particle-particle-mesh ($\mathrm{P^3M}$) methods [29].

The fast multipole expansion [25] method allows the computation of some characteristics of the multiparticle potential, say, the interaction energy, at the expense $O(N \log N)$ by evaluation of the potential only at N sampling points x_ν.

Computation of long-range interaction potentials of large many-particle systems is discussed, for example, in [15, 43, 50], and in [29, 1, 19, 20, 56, 23] using grid-based approaches. Ewald-type splitting of the Coulomb interaction into long- and short-range components is applied in density functional theory calculations in [55].

In this paper, we introduce and analyze the new range-separated (RS) canonical/Tucker tensor format which aims for the efficient numerical treatment of 3D long-range interaction potentials in a system of generally distributed particles. The main idea of the RS format is the independent grid-based low-rank tensor representation to the long- and short-range parts in the total sum of single-particle (say, electrostatic) potentials in (1.1) discretized on a fine 3D $n \times n \times n$ Cartesian grid Ω_n in the computational box $\Omega \in \mathbb{R}^3$. Such a representation is based on the splitting of a single reference potential e.g., $p(\|x\|) = 1/\|x\|$, into a sum of localized and long-range, low-rank canonical tensors that are both represented on the computational grid Ω_n.

The main advantage of the RS format is the efficient representation of the long-range contributions to the total potential sum in (1.1) by using the multigrid accelerated canonical-to-Tucker transform [39], which returns this part in the form of a low-rank canonical/Tucker tensor at the asymptotical cost $O(N n)$. In Theorem 3.1, we prove that the corresponding tensor rank only weakly (logarithmically) depends on the number of particles N. Hence, the long-range contribution to the target sum is represented via the low-rank global canonical/Tucker tensor defined on the fine $n \times n \times n$ grid Ω_n in the $O(n)$ storage. These features are demonstrated by numerical tests for the large 3D clusters of generally distributed particles.

In turn, the short-range contribution to the total sum is constructed by using a *single* reference low-rank tensor of local support selected from the "short-range" canonical vectors in the tensor decomposition of $p(\|x\|)$. To that end, the whole set of N short-range clusters is represented by replication and rescaling of the small-size localized canonical tensor defined on an $n_s \times n_s \times n_s$ Cartesian grid with $n_s \ll n$, thus reducing the storage to the $O(1)$-parametrization of the reference canonical tensor and the list of coordinates and charges of particles. Summation of the short-range part

over an $n \times n \times n$ grid needs $O(N\, n_s)$ computational work for an N-particle system. Such a cumulated sum of the short-range components allows *local* operations in the RS canonical format, making it particularly efficient for tensor multilinear algebra.

The particular benefit of the RS approach is the low-parametric representation of the collective interaction potential on a large 3D Cartesian grid in the whole computational domain Ω at the linear cost $O(n)$, thus outperforming the traditional grid-based summation techniques based on the full-grid $O(n^3)$-representation in the volume. Both global and local summation schemes are quite easy in program implementation. The prototype algorithms in MATLAB applied on a laptop enable computation of the RS-tensor representation of electrostatic potentials for large many-particle systems on fine grids of size up to $n^3 = 10^{12}$.

The efficient numerical realization of RS formats can be achieved by a trade-off between the rank parameters in the long-range part and the effective support of the local subtensors. Indeed, the range separation step can be realized *adaptively* by simple tuning of the splitting rank parameters in the reference tensor based on an ε-tolerance threshold in estimating the effective local support. The low-rank RS canonical/Tucker tensor representation simplifies further operations on the resultant interaction potential (for example, 3D integration, computation of gradients and forces, and evaluation of the interaction energy of a system) by reducing all of them to 1D calculations.

As one of many possible applications of the RS tensor format, we propose a new numerical scheme for calculating the free interaction energy of proteins. We also demonstrate that the RS tensor formats can be useful for the numerical modeling of multidimensional scattered data by means of the efficient data sparse approximation to the "inter-distance" matrix via the short-term sum of Kronecker product matrices with "univariate" factors.

The RS tensor format was motivated by the recent method for efficient summation of the long-range electrostatic potentials on large lattices with defects, which uses the assembled canonical and Tucker tensors [32, 34] which provides a competitive alternative to the Ewald summation schemes [22]. In the case of 3D finite lattice systems, the grid-based tensor summation technique yields asymptotic complexity $O(N^{1/3})$ in the number of particles N, and almost linear complexity in the univariate grid size n.

The RS tensor approach can be interpreted as the model reduction based on low-rank tensor approximations (i.e., via a small number of representation parameters). The model reduction techniques for PDEs and control problems have been described in detail in [7, 51, 4].

In recent years, tensor numerical methods have been recognized as a powerful tool in scientific computing for multidimensional problems; see, for example, [37, 24, 33, 6, 2] and [18, 17, 52, 42, 27, 13, 3]. In particular, the approximating properties of tensor decompositions in the modeling of high-dimensional problems have been addressed in [54, 11, 26, 14]. Here we notice that, in the case of higher dimensions, the local canonical tensors can be combined with the global low-rank tensor train (TT) representation [49], thus introducing the RS-TT format; see Remark 3.12.

The rest of the paper is organized as follows. In section 2, we recall the rank-structured canonical and Tucker tensor formats, and discuss the representation of a radial basis function by a canonical tensor approximation via sinc-quadratures for the Laplace transform. Section 2.3 describes the principles of short- and long-range splitting of the generating kernel on example of the 3D electrostatic potential, which leads to the new concept of the RS tensor format. In section 3, we introduce and analyze range-separated (RS) tensor formats. Section 3.1 demonstrates that the long-range

part of the total potential sum of a large number of particles exhibits low canonical rank. In particular, Theorem 3.1 proves that the Tucker rank of the long-range part in the total potential sum only logarithmically depends on the number of particles involved. The cumulated representation of the short-range part of the total potential is described in section 3.3, where the RS canonical and Tucker tensor formats are defined. In section 4, we discuss how the RS tensor formats can be utilized in the numerical treatment of multidimensional scattered data, and in the calculation of the free interaction energy of protein-type systems. We refer to the extended preprint version of this paper [5], where further possible applications have been discussed.

2. Low-rank tensor splitting for multivariate generating kernels. In this section, we introduce the RS low-rank tensor splitting for the multivariate radial basis functions, which will be the important ingredient in the construction of the RS tensor formats.

2.1. Rank-structured tensor formats. Here we recall the commonly used rank-structured tensor formats[1] utilized in this paper (see also the literature surveys [41, 37, 24]). The traditional canonical and Tucker tensor representations have long been employed in computer science for the quantitative analysis of correlations in multidimensional data arising in image processing, chemometrics, psychometrics etc.; see [16, 41] and references therein.

These classical tensor formats recently attracted attention in scientific computing when it was numerically demonstrated and rigorously proved that the class of function-related tensors[2] allows low-rank tensor-structured decomposition [35, 38]. In particular, such tensor approximations proved to be efficient for real-space calculations in computational quantum chemistry [32, 33].

A tensor of order d is defined as a multidimensional array over a d-tuple index set

$$\mathbf{A} = [a_{i_1,\dots,i_d}] \equiv [a(i_1,\dots,i_d)] \ \in \mathbb{R}^{n_1\times\cdots\times n_d} \ \text{ with } \quad i_\ell \in I_\ell := \{1,\dots,n_\ell\},$$

considered as an element of a linear vector space equipped with the Euclidean scalar product. A tensor with all dimensions having equal size $n_\ell = n$, $\ell = 1,\dots d$, will be called an $n^{\otimes d}$ tensor. The required storage size scales exponentially in the dimension n^d, which results in the so-called "curse of dimensionality."

To get rid of exponential scaling in the dimension, one can apply the rank-structured separable representations (approximations) of multidimensional tensors. The simplest separable element is given by the rank-1 tensor

$$\mathbf{U} = \mathbf{u}^{(1)} \otimes \cdots \otimes \mathbf{u}^{(d)} \in \mathbb{R}^{n_1\times\cdots\times n_d}$$

with entries $u_{i_1,\dots,i_d} = u^{(1)}_{i_1},\dots,u^{(d)}_{i_d}$, requiring only $n_1+\cdots+n_d$ numbers to store it. A tensor in the R-term canonical format is defined by a finite sum of rank-1 tensors

$$\mathbf{U} = \sum\nolimits_{k=1}^{R} \xi_k \mathbf{u}^{(1)}_k \otimes \cdots \otimes \mathbf{u}^{(d)}_k, \quad \xi_k \in \mathbb{R}, \tag{2.1}$$

[1] The commonly used notion of *rank-structured tensor formats* for the compressed representation of multidimensional data is usually understood in the sense of (nonlinear) parametrization by a small number of parameters that allows for low storage costs, a simple representation of each entry in the target data array, and efficient, "formatted" multilinear algebra via reduction to univariate operations.

[2] Function-related tensors are obtained by sampling the multivariate function $f = f(x_1,\dots,x_d)$ defined on the hypercube $f : [0,1]^d \to \mathbb{R}$ onto the tensor grid of size $n_1\times\cdots\times n_d$. As a result, the function is approximated by the d-dimensional tensor array $f \approx \mathbf{F} \in \mathbb{R}^{n_1\times\cdots\times n_d}$. The target function f can also be given as a large sum of separable functions, say Gaussians.

where $\mathbf{u}_k^{(\ell)} \in \mathbb{R}^{n_\ell}$ are normalized vectors, and R is called the canonical rank of a tensor. Now the storage cost is bounded by dRn. For $d \geq 3$, there are no algorithms for the computation of the canonical rank of a tensor $\mathbf{U}$, i.e., the minimal number R in representation (2.1) and the respective decomposition with the polynomial cost in d.

We say that a tensor $\mathbf{V}$ is represented in the rank-$\mathbf{r}$ orthogonal Tucker format with the rank parameter $\mathbf{r} = (r_1, \dots, r_d)$ if

$$\mathbf{V} = \sum_{\nu_1=1}^{r_1} \dots \sum_{\nu_d=1}^{r_d} \beta_{\nu_1,\dots,\nu_d}\, \mathbf{v}_{\nu_1}^{(1)} \otimes \dots \otimes \mathbf{v}_{\nu_d}^{(d)} \equiv \boldsymbol{\beta} \times_1 V^{(1)} \times_2 V^{(2)} \cdots \times_d V^{(d)}, \tag{2.2}$$

where $\{\mathbf{v}_{\nu_\ell}^{(\ell)}\}_{\nu_\ell=1}^{r_\ell} \in \mathbb{R}^{n_\ell}$ represents a set of orthonormal vectors for $\ell = 1, \dots, d$, $\times_\ell$ denotes the contraction along the mode ℓ with the orthogonal matrices $V^{(\ell)} = [\mathbf{v}_1^{(\ell)}, \dots, \mathbf{v}_{r_\ell}^{(\ell)}] \in \mathbb{R}^{n_\ell \times r_\ell}$, and $\boldsymbol{\beta} = [\beta_{\nu_1,\dots,\nu_d}] \in \mathbb{R}^{r_1 \times \dots \times r_d}$ is the Tucker core tensor. The storage cost for the Tucker tensor is bounded by $drn + r^d$ with $r = |\mathbf{r}| := \max_\ell r_\ell$.

The representation (2.1) can be written as the rank-$(R, \dots, R)$ (nonorthogonal) Tucker tensor

$$\mathbf{U} = \boldsymbol{\xi} \times_1 U^{(1)} \times_2 U^{(2)} \cdots \times_d U^{(d)}, \tag{2.3}$$

by introducing the so-called side matrices $U^{(\ell)} = [\mathbf{u}_1^{(\ell)}, \dots, \mathbf{u}_R^{(\ell)}] \in \mathbb{R}^{n_\ell \times R}$, $\ell = 1, \dots, d$, obtained by concatenation of the canonical vectors $\mathbf{u}_k^{(\ell)}$, $k = 1, \dots, R$, and the diagonal Tucker core tensor $\boldsymbol{\xi} := \mathrm{diag}\{\xi_1, \dots, \xi_R\} \in \mathbb{R}^{R \times \dots \times R}$ such that $\xi_{\nu_1,\dots,\nu_d} = 0$ except when $\nu_1 = \dots = \nu_d$ with $\xi_{\nu,\dots,\nu} = \xi_\nu$ $(\nu = 1, \dots, R)$.

In the case $d = 2$, the orthogonal Tucker decomposition is equivalent to the singular value decomposition (SVD) of a rectangular matrix, while the canonical representation corresponds to the rank-R skeleton decomposition of a matrix.

The exceptional properties of the Tucker decomposition for the approximation of discretized multidimensional functions have been revealed in [35, 38], where it was proven that for a class of function-related tensors the approximation error of the Tucker decomposition decays exponentially in the Tucker rank.

Rank-structured tensor representations provide fast multilinear algebra with linear complexity scaling in the dimension d. For example, for given canonical tensors (2.1), the Euclidean scalar product, the Hadamard product, and d-dimensional convolution can be computed by univariate tensor operations in 1D complexity [38]. In tensor-structured numerical methods, calculation of the d-dimensional convolution integrals is replaced by a sequence of 1D scalar and Hadamard products, and 1D convolution transforms [39, 38], leading to $O(dn \log n)$ computational work instead of $O(n^d)$. However, the multilinear tensor operations in the above-mentioned formats necessarily lead to an increase of the tensor ranks, which can then be reduced by the canonical-to-Tucker and Tucker-to-canonical algorithms introduced in [38, 39]; see the extended preprint [5] for a detailed description.

2.2. Canonical tensor representation of the multivariate generating kernel. Methods of separable approximation to the 3D Newton kernel (electrostatic potential) using the Gaussian sums have been addressed in the chemical and mathematical literature since [10] and [54, 11, 26], respectively. The approach to tensor decomposition for a class of lattice-structured interaction potentials $p(\|x\|)$ was presented in [32, 34]. In this section, we recall the grid-based method for the low-rank canonical representation of a spherically symmetric kernel function $p(\|x\|)$, $x \in \mathbb{R}^d$ for $d = 2, 3, \dots$, by its projection onto the set of piecewise constant basis functions; see

[8] for the case of Newton and Yukawa kernels $p(\|x\|) = \frac{1}{\|x\|}$ and $p(\|x\|) = \frac{e^{-\lambda\|x\|}}{\|x\|}$ for $x \in \mathbb{R}^3$. The single reference potential, like $1/\|x\|$, can be represented on a fine 3D $n \times n \times n$ Cartesian grid in the form of a low-rank canonical tensor [26, 8]. Further, we confine ourselves to the case $d = 3$.

In the computational domain $\Omega = [-b, b]^3$, let us introduce the uniform $n \times n \times n$ rectangular Cartesian grid Ω_n with mesh size $h = 2b/n$ (n even). Let $\{\psi_{\mathbf{i}}\}$ be a set of tensor-product piecewise constant basis functions, $\psi_{\mathbf{i}}(\mathbf{x}) = \prod_{\ell=1}^{3} \psi_{i_\ell}^{(\ell)}(x_\ell)$, for the 3-tuple index $\mathbf{i} = (i_1, i_2, i_3)$, $i_\ell \in I_\ell = \{1, \ldots, n\}$, $\ell = 1, 2, 3$. The generating kernel $p(\|x\|)$ is discretized by its projection onto the basis set $\{\psi_{\mathbf{i}}\}$ in the form of a third-order tensor of size $n \times n \times n$, defined entrywise as

$$\mathbf{P} := [p_{\mathbf{i}}] \in \mathbb{R}^{n\times n\times n}, \quad p_{\mathbf{i}} = \int_{\mathbb{R}^3} \psi_{\mathbf{i}}(x) p(\|x\|)\, \mathrm{d}x. \tag{2.4}$$

The low-rank canonical decomposition of the third-order tensor $\mathbf{P}$ is based on the use of exponentially convergent sinc-quadratures for approximating the Laplace–Gauss transform to the analytic function $p(z)$, $z \in \mathbb{C}$, specified by a certain weight $a(t) > 0$:

$$p(z) = \int_{\mathbb{R}_+} a(t) e^{-t^2 z^2}\, \mathrm{d}t \approx \sum_{k=-M}^{M} a_k e^{-t_k^2 z^2} \quad \text{for} \quad |z| > 0, \quad z \in \mathbb{R}, \tag{2.5}$$

where the quadrature points and weights are given by

$$t_k = k\mathfrak{h}_M, \quad a_k = a(t_k)\mathfrak{h}_M, \quad \mathfrak{h}_M = C_0 \log(M)/M, \quad C_0 > 0. \tag{2.6}$$

Under the assumption $0 < a \le |z| < \infty$, this quadrature can be proven to provide an exponential convergence rate in M for a class of analytic functions $p(z)$. The sinc–quadrature based approximation to the generating function by using the short-term Gaussian sums in (2.5), (2.6) is applicable to the class of analytic functions in a certain strip $|z| \le D$ of the complex plane, such that on the real axis these functions decay polynomially or exponentially. We refer to basic results in [54, 11, 26], where the exponential convergence of the sinc-approximation in the number of terms (i.e., the canonical rank) was analyzed.

Now, for any fixed $x = (x_1, x_2, x_3) \in \mathbb{R}^3$ such that $\|x\| > a > 0$, we apply the sinc-quadrature approximation (2.5), (2.6) to obtain the separable expansion

$$p(\|x\|) = \int_{\mathbb{R}_+} a(t) e^{-t^2\|x\|^2}\, \mathrm{d}t \approx \sum_{k=-M}^{M} a_k e^{-t_k^2\|x\|^2} = \sum_{k=-M}^{M} a_k \prod_{\ell=1}^{3} e^{-t_k^2 x_\ell^2}, \tag{2.7}$$

providing an exponential convergence rate in M:

$$\left| p(\|x\|) - \sum_{k=-M}^{M} a_k e^{-t_k^2\|x\|^2} \right| \le \frac{C}{a}\, e^{-\beta\sqrt{M}} \quad \text{with some } C, \beta > 0. \tag{2.8}$$

Combining (2.4) and (2.7), and taking into account the separability of the Gaussian basis functions, we arrive at the low-rank approximation to each entry of the tensor $\mathbf{P}$:

$$p_{\mathbf{i}} \approx \sum_{k=-M}^{M} a_k \int_{\mathbb{R}^3} \psi_{\mathbf{i}}(x) e^{-t_k^2\|x\|^2} \mathrm{d}x = \sum_{k=-M}^{M} a_k \prod_{\ell=1}^{3} \int_{\mathbb{R}} \psi_{i_\ell}^{(\ell)}(x_\ell) e^{-t_k^2 x_\ell^2} \mathrm{d}x_\ell.$$

Define the vector (recall that $a_k > 0$)

$$\mathbf{p}_k^{(\ell)} = a_k^{1/3} \left[b_{i_\ell}^{(\ell)}(t_k) \right]_{i_\ell=1}^{n_\ell} \in \mathbb{R}^{n_\ell} \quad \text{with} \quad b_{i_\ell}^{(\ell)}(t_k) = \int_{\mathbb{R}} \psi_{i_\ell}^{(\ell)}(x_\ell) e^{-t_k^2 x_\ell^2} \mathrm{d}x_\ell;$$

then the third-order tensor $\mathbf{P}$ can be approximated by the R-term ($R = 2M + 1$) canonical representation

$$\mathbf{P} \approx \mathbf{P}_R = \sum_{k=-M}^{M} a_k \bigotimes_{\ell=1}^{3} \mathbf{b}^{(\ell)}(t_k) = \sum_{k=-M}^{M} \mathbf{p}_k^{(1)} \otimes \mathbf{p}_k^{(2)} \otimes \mathbf{p}_k^{(3)} \in \mathbb{R}^{n \times n \times n}, \tag{2.9}$$

where $\mathbf{p}_k^{(\ell)} \in \mathbb{R}^n$. Given a threshold $\varepsilon > 0$, M can be chosen as the minimal number such that in the max-norm,

$$\|\mathbf{P} - \mathbf{P}_R\| \le \varepsilon \|\mathbf{P}\|.$$

The skeleton vectors can be renumerated by $k \mapsto q = k + M + 1$, $\mathbf{p}_k^{(\ell)} \mapsto \mathbf{p}_q^{(\ell)}$ ($q = 1, \dots, R$), $\ell = 1, 2, 3$. The canonical tensor $\mathbf{P}_R$ in (2.9) approximates the 3D symmetric kernel function $p(\|x\|)$, $x \in \Omega$, centered at the origin such that $\mathbf{p}_q^{(1)} = \mathbf{p}_q^{(2)} = \mathbf{p}_q^{(3)}$ ($q = 1, \dots, R$).

In the case of the Newton kernel, we have $p(z) = 1/z$, and the Laplace–Gauss transform representation takes the form

$$\frac{1}{z} = \frac{2}{\sqrt{\pi}} \int_{\mathbb{R}_+} e^{-z^2 t^2} dt, \quad \text{where} \quad z = \sqrt{x_1^2 + x_2^2 + x_3^2}.$$

In this case, the term $\mathbf{p}_k^{(\ell)}$ equals $\mathbf{p}_{-k}^{(\ell)}$, and the sum (2.9) reduces to $k = 0, 1, \dots, M$, implying $R = M + 1$. Figure 1 displays the canonical vectors in the symmetric tensor representation (2.9) for the Newton kernel along the x-axis from a set $\{\mathbf{p}_q^{(1)}\}_{q=1}^R$. It can be clearly seen that there are canonical vectors representing the long- and short-range contributions to the total electrostatic potential. This interesting feature was also recognized for the rank-structured tensors representing a lattice sum of electrostatic potentials [32, 34].

2.3. Tensor splitting of the kernel into long- and short-range parts. From the definition of the quadrature (2.9), (2.6), we can easily observe that the full set of approximating Gaussians includes two classes of functions: those with small "effective support" and the long-range functions. Consequently, functions from different classes may require different tensor-based schemes for efficient numerical

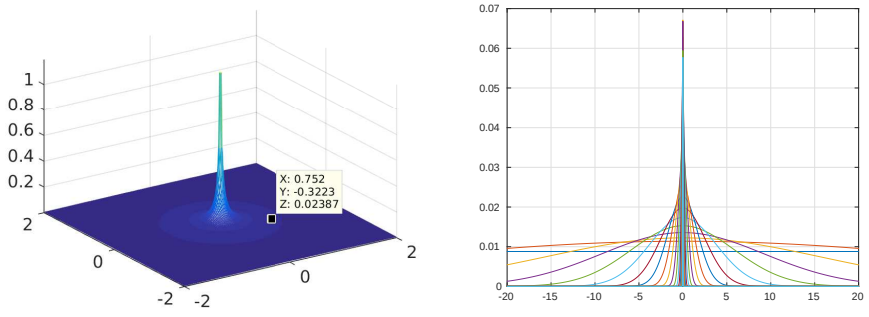

FIG. 1. *Vectors of the canonical tensor representation* $\{\mathbf{p}_q^{(1)}\}_{q=1}^R$ *for the Newton kernel displayed along the* x*-axis:* $n = 1024$, $R = 20$.

treatment. Hence, the idea of the new approach is the constructive implementation of a range separation scheme that allows the independent efficient treatment of both the long- and short-range parts in each summand in (1.1).

In what follows, without loss of generality, we confine ourselves to the case of the Newton kernel, so that the sum in (2.9) reduces to $k = 0, 1, \dots, M$ (due to the symmetry argument). From (2.6) we observe that the sequence of quadrature points $\{t_k\}$ can be split into two subsequences $\mathcal{T} := \{t_k | k = 0, 1, \dots, M\} = \mathcal{T}_l \cup \mathcal{T}_s$ with

$$\mathcal{T}_l := \{t_k \,| k = 0, 1, \dots, R_l\} \quad \text{and} \quad \mathcal{T}_s := \{t_k \,| k = R_l + 1, \dots, M\}. \tag{2.10}$$

Here $\mathcal{T}_l$ includes quadrature points t_k condensed "near" zero, hence generating the long-range Gaussians (low-pass filters), and $\mathcal{T}_s$ accumulates the increasing in $M \to \infty$ sequence of "large" sampling points t_k with the upper bound $C_0^2 \log^2(M)$, corresponding to the short-range Gaussians (high-pass filters). Notice that the quasi-optimal choice of the constant $C_0 \approx 3$ was determined in [8]. We futher denote $\mathcal{K}_l := \{k \,| k = 0, 1, \dots, R_l\}$ and $\mathcal{K}_s := \{k \,| k = R_l + 1, \dots, M\}$.

Splitting (2.10) generates the additive decomposition of the canonical tensor $\mathbf{P}_R$ onto the short- and long-range parts,

$$\mathbf{P}_R = \mathbf{P}_{R_s} + \mathbf{P}_{R_l},$$

where

$$\mathbf{P}_{R_s} = \sum_{t_k \in \mathcal{T}_s} \mathbf{p}_k^{(1)} \otimes \mathbf{p}_k^{(2)} \otimes \mathbf{p}_k^{(3)}, \quad \mathbf{P}_{R_l} = \sum_{t_k \in \mathcal{T}_l} \mathbf{p}_k^{(1)} \otimes \mathbf{p}_k^{(2)} \otimes \mathbf{p}_k^{(3)}. \tag{2.11}$$

The choice of the critical number $R_l = \#\mathcal{T}_l - 1$ (or, equivalently, $R_s = \#\mathcal{T}_s = M - R_l$) that specifies the splitting $\mathcal{T} = \mathcal{T}_l \cup \mathcal{T}_s$ is determined by the *active support* of the short-range components, such that one can cut off the functions $\mathbf{p}_k(x)$, $t_k \in \mathcal{T}_s$ outside of the sphere B_σ of the radius $\sigma > 0$ subject to a certain threshold $\delta > 0$. For fixed $\delta > 0$, the choice of R_s is uniquely defined by the (small) parameter σ and vice versa. Given σ, the following two basic criteria, corresponding to (A) the max-norm and (B) the L^1-norm estimates, can be applied:

$$\text{(A)} \quad \mathcal{T}_s = \{t_k : a_k e^{-t_k^2 \sigma^2} \le \delta\} \;\Leftrightarrow\; R_l = \min k : a_k e^{-t_k^2 \sigma^2} \le \delta, \tag{2.12}$$

$$\text{(B)} \quad \mathcal{T}_s := \left\{ t_k : a_k \int_{B_\sigma} e^{-t_k^2 x^2} dx \le \delta \right\} \;\Leftrightarrow\; R_l = \min k : a_k \int_{B_\sigma} e^{-t_k^2 x^2} dx \le \delta. \tag{2.13}$$

The quantitative estimates on the value of R_l can be easily calculated by using the explicit equation (2.6) for the quadrature parameters. For example, in the case $C_0 = 3$ and $a(t) = 1$, criterion (A) implies that R_l solves the equation

$$\left(\frac{3 R_l \log M}{M} \right)^2 \sigma^2 = \log \left(\frac{\mathfrak{h}_M}{\delta} \right).$$

Criteria (2.12) and (2.13) can be modified depending on the particular applications. For example, in electronic structure calculations, the parameter σ can be associated with the typical interatomic distance in the molecular system of interest.

Figure 2 illustrates the splitting (2.10) for the tensor $\mathbf{P}_R = \mathbf{P}_{R_l} + \mathbf{P}_{R_s}$ in (2.11) represented on the $n \times n \times n$ grid with the parameters $R = 20, R_l = 12$, and $R_s = 8$,

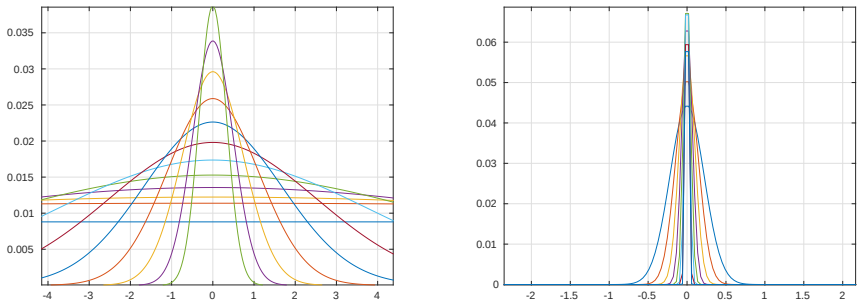

FIG. 2. *Long- and short-range canonical vectors for* $n = 1024$, $R = 20$, *and* $R_l = 12$.

respectively. Following criterion (A) with $\delta \approx 10^{-4}$, the effective support for this splitting is determined by $\sigma = 0.9$. The complete Newton kernel depicted in Figure 1 covers the long-range behavior, while the function values of the tensor $\mathbf{P}_{R_s}$ vanish exponentially fast apart of the effective support; see the right panel of Figure 2.

Inspection of the quadrature point distribution in (2.6) shows that the short- and long-range subsequences are nearly equally balanced distributed, so one can expect approximately

$$R_s \approx R_l = M/2. \tag{2.14}$$

The optimal choice may depend on the particular kernel function and the specific applications.

The advantage of range separation in the splitting of the canonical tensor $\mathbf{P}_R \mapsto \mathbf{P}_{R_s} + \mathbf{P}_{R_l}$ in (2.11) is the opportunity to obtain independent tensor representations of both subtensors $\mathbf{P}_{R_s}$ and $\mathbf{P}_{R_l}$, providing the separate treatment of the short- and long-range parts in the total sum of many-interaction potentials as in (1.1).

Finally, we notice that the *range separation principle* can be generalized to more than two-term splitting, taking into account the requirements of specific applications.

3. Range-separated tensor format for modeling the multiparticle potentials. Given the generating kernel $p(\|x\|)$, we consider the problem of efficiently calculating the weighted sum of a large number of single potentials located in a set $\mathcal{S}$ of separable distributed points (sources) $x_\nu \in \mathbb{R}^3$, $\nu = 1, \dots, N$, embedded in the fixed bounding box $\Omega = [-b, b]^3$,

$$P_0(x) = \sum_{\nu=1}^{N} z_\nu \, p(\|x - x_\nu\|), \quad z_\nu \in \mathbb{R}, \quad x, x_\nu \in \Omega, \tag{3.1}$$

where the radial basis function $p(\|x\|)$ is allowed to have slow polynomial decay in $1/\|x\|$ so that each individual source contributes essentially to the total potential at each point in Ω.

In what follows, for ease of presentation, we confine ourselves to the case of electrostatic potentials described by the Newton kernel $p(\|x\|) = \frac{1}{\|x\|}, x \in \mathbb{R}^3$.

3.1. Low-rank representation to the sum of long-range terms. First, we describe the tensor summation method for calculation of the collective potential of a multiparticle system that includes only the long-range contribution from the generating kernel.

We introduce the $n \times n \times n$ rectangular grid Ω_n in $\Omega = [-b, b]^3$ (see section 2.2) as well as the auxiliary $2n \times 2n \times 2n$ grid $\widetilde{\Omega}_{2n}$ on the accompanying domain $\widetilde{\Omega} = 2\Omega$ of double size. The canonical rank-R representation of the Newton kernel on $\widetilde{\Omega}_{2n}$, living on the extended index set $\widetilde{I}$, and its restriction onto the $n \times n \times n$ subgrid are denoted by $\widetilde{\mathbf{P}}_R$ and $\mathbf{P}_R \in \mathbb{R}^{n\times n\times n}$, respectively; see (2.9).

Consider the splitting (2.11) applied to the reference canonical tensor $\mathbf{P}_R$ and to its accompanying version $\widetilde{\mathbf{P}}_R = [\widetilde{p}_R(i_1, i_2, i_3)]$, $i_\ell \in \widetilde{I}_\ell$, $\ell = 1, 2, 3$, such that

$$\widetilde{\mathbf{P}}_R = \widetilde{\mathbf{P}}_{R_s} + \widetilde{\mathbf{P}}_{R_l} \in \mathbb{R}^{2n\times 2n\times 2n}.$$

For technical reasons, we further assume that the tensor grid Ω_n is fine enough, such that all charge centers $\mathcal{S} = \{x_\nu\}$ specifying the total electrostatic potential in (3.1) belong to the set of grid points, i.e., $x_\nu = (x_{\nu,1}, x_{\nu,2}, x_{\nu,3})^T = h(j_1^{(\nu)}, j_2^{(\nu)}, j_3^{(\nu)})^T \in \Omega_n$ with some indexes $1 \le j_1^{(i)}, j_2^{(i)}, j_3^{(i)} \le n$.

The total electrostatic potential $P_0(x)$ in (3.1) is represented by a projected tensor $\mathbf{P}_0 \in \mathbb{R}^{n\times n\times n}$ that can be constructed by a direct sum of shift-and-windowing transforms of the reference tensor $\widetilde{\mathbf{P}}_R$ (see [32] for more details):

$$\mathbf{P}_0 = \sum_{\nu=1}^{N} z_\nu \, \mathcal{W}_\nu(\widetilde{\mathbf{P}}_R) = \sum_{\nu=1}^{N} z_\nu \, \mathcal{W}_\nu(\widetilde{\mathbf{P}}_{R_s} + \widetilde{\mathbf{P}}_{R_l}) =: \mathbf{P}_s + \mathbf{P}_l. \tag{3.2}$$

The shift-and-windowing transform $\mathcal{W}_\nu$ maps a reference tensor $\widetilde{\mathbf{P}}_R \in \mathbb{R}^{2n\times 2n\times 2n}$ onto its subtensor of smaller size $n \times n \times n$, which is obtained by first shifting the center of the reference tensor $\widetilde{\mathbf{P}}_R$ to the grid point x_ν and then restricting (windowing) the result onto the computational grid Ω_n:

$$\mathcal{W}_\nu : \widetilde{\mathbf{P}}_R \mapsto \mathbf{P}^{(\nu)} = [p^{(\nu)}_{i_1,i_2,i_3}], \quad p^{(\nu)}_{i_1,i_2,i_3} := \widetilde{p}_R(i_1 + j_1^{(\nu)}, i_2 + j_2^{(\nu)}, i_3 + j_3^{(\nu)}), \quad i_\ell \in I_\ell.$$

The point is that the number of terms in the canonical representation of the full tensor sum $\mathbf{P}_0$ increases almost proportionally to the number N of particles in the system. Figure 3 demonstrates singular values of the side matrix in the canonical tensor $\mathbf{P}_0$. Furthermore, the compressed canonical rank of the tensor $\mathbf{P}_0$ shows up the pessimistic bound $\le R\,N$.

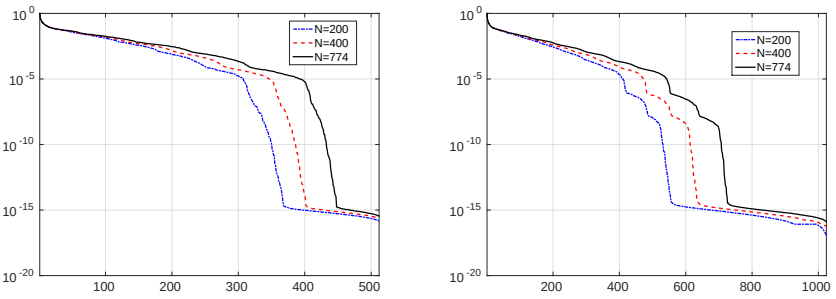

FIG. 3. *Mode-1 singular values of the side matrix in the canonical representation of the total potential sum* $\mathbf{P}_0$ *versus the number of particles* $N = 200, 400, 774$ *and grid size* n*:* $n = 512$ *(left);* $n = 1024$ *(right).*

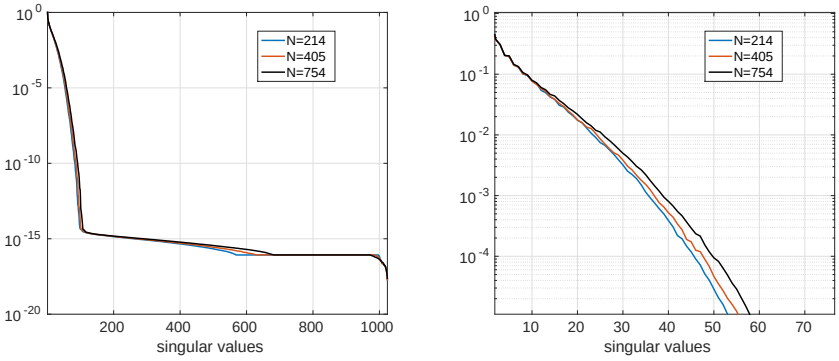

FIG. 4. *Mode-1 singular values of side matrices for the long-range part* $\mathbf{P}_l$ *(with* $R_l = 12$*) in the total potential versus the number of particles* N *(left). Zoom of the first* 70 *singular values (right).*

To overcome this difficulty, in what follows we consider the global tensor decomposition of only the *long-range* part in the tensor $\mathbf{P}_0$, defined by

$$\mathbf{P}_l = \sum_{\nu=1}^{N} z_\nu \, \mathcal{W}_\nu(\widetilde{\mathbf{P}}_{R_l}) = \sum_{\nu=1}^{N} z_\nu \, \mathcal{W}_\nu \left(\sum_{k \in \mathcal{K}_l} \widetilde{\mathbf{p}}_k^{(1)} \otimes \widetilde{\mathbf{p}}_k^{(2)} \otimes \widetilde{\mathbf{p}}_k^{(3)} \right). \tag{3.3}$$

Since by construction the tensor $\mathbf{P}_l$ approximates rather smooth functions on the domain Ω, one may expect that the large initial rank can be reduced considerably to some value $R_* \ll RN$ that remains almost independent of N. The principal ingredient of our tensor approach is the rank reduction in the initial large canonical sum $\mathbf{P}_l$ by application of the multigrid accelerated canonical-to-Tucker (C2T) transform. The first step in the C2T transform is the SVD of side matrices $U^{(\ell)}$, $\ell = 1, 2, 3$, in the initial canonical tensor of type (2.3) (the so-called reduced higher order singular value decomposition [RHOSVD]; see [39]).

The left panel of Figure 4 illustrates that the singular values of the side matrices for the long-range part exhibit fast exponential decay with a rate independent of $N = 214, 405$, and 754 (cf. Figure 3). The right panel of Figure 4 zooms into the first 50 singular values, which are almost identical for the different values of N. The fast decay in singular values guarantees the existence of low-rank RHOSVD-based Tucker decomposition (see [5]) to the long-range part $\mathbf{P}_l$.

The following theorem justifies the above observations and proves that the Tucker ε-rank of the long-range part in the accumulated sum of potentials in the bounding box $\Omega = [-b, b]^3$ remains almost independent of the number of particles N (but depends on the domain size b). Simplifying the exposition, we assume that the tensor entries in $\mathbf{P}_l$ are computed by collocation of Gaussian sums at the centers of the grid-cells. This provides a representation which is practically identical to that of (2.9).

THEOREM 3.1. *Let the long-range part* $\mathbf{P}_l$ *in the total interaction potential (see* (3.3)*) correspond to the choice of the splitting parameter in* (2.14) *with* $M = O(\log^2 \varepsilon)$*. Then the total* ε*-rank* $\mathbf{r}_0$ *of the Tucker approximation to the canonical tensor sum* $\mathbf{P}_l$ *is bounded by*

$$|\mathbf{r}_0| := \mathrm{rank}_{Tuck}(\mathbf{P}_l) = C\, b\, \log^{3/2}(|\log(\varepsilon/N)|),$$

where the constant C *does not depend on the number of particles* N*.*

Proof. We consider the Gaussian in normalized form $G_\sigma(x) = \mathrm{e}^{-\frac{x^2}{2\sigma^2}}$ so that the relation $\mathrm{e}^{-t_k^2 x^2} = \mathrm{e}^{-\frac{x^2}{2\sigma^2}}$ holds, i.e., we set (see (2.6))

$$t_k = \frac{1}{\sqrt{2}\sigma_k} \quad \text{with } t_k = k\mathfrak{h}_M, \quad k = 0, 1, \ldots, M,$$

where $\mathfrak{h}_M = C_0 \log M/M$. The choice of R_s is based on criterion (B) in (2.13) on the bound of the L^1-norm, which reads

$$a_k \int_a^\infty \mathrm{e}^{-\frac{x^2}{2\sigma_k^2}} \le \frac{\varepsilon}{2} < 1, \quad a_k = \mathfrak{h}_M.$$

This allows us to select all σ_k, which satisfy this criteria.

We sketch the proof according to the following steps. (a) We represent all shifted Gaussian functions, contributing to the total sum in the fixed set of basis functions by using a truncated Fourier series. (b) We prove that, on the "long-range" index set $k \in \mathcal{T}_l$, the parameter σ_k remains uniformly bounded in N from below, implying the uniform bound on the number of terms in the ε-truncated Fourier series. (c) The summation of functions presented in the fixed Fourier basis set does not enlarge the Tucker rank, but only effects the Tucker core. The dependence on size of computational domain b appears in the explicit form.

Specifically, let us consider the rank-1 term in the splitting (2.11) with maximal index $k \in \mathcal{T}_l$. Taking into account the asymptotic choice $M = \log^2 \varepsilon$ (see (2.8)) where $\varepsilon > 0$ is the accuracy of the sinc-quadrature, the relation (2.14) implies

$$\max_{k \in \mathcal{T}_l} t_k = R_l \mathfrak{h}_M = \frac{M}{2} C_0 \log(M)/M \approx \log(M) = 2\log(|\log(\varepsilon)|). \tag{3.4}$$

Now we consider the Fourier transform of the univariate Gaussian on $[-b, b]$:

$$G_\sigma(x) = \mathrm{e}^{-\frac{x^2}{2\sigma^2}} = \sum_{m=0}^{M} \alpha_m \cos\Big(\frac{\pi m x}{b}\Big) + \eta \quad \text{with} \quad |\eta| = \left| \sum_{m=M+1}^{\infty} \alpha_m \cos\Big(\frac{\pi m x}{b}\Big) \right| < \varepsilon,$$

where

$$\alpha_m = \frac{\displaystyle\int_{-b}^{b} \mathrm{e}^{-\frac{x^2}{2\sigma^2}} \cos\Big(\frac{\pi m x}{b}\Big)\, dx}{|C_m|^2} \quad \text{with} \quad |C_m|^2 = \int_{-b}^{b} \cos^2\Big(\frac{\pi m x}{b}\Big)\, dx = \begin{cases} 2b & \text{if } m = 0, \\ b & \text{otherwise.} \end{cases}$$

Following arguments in [21] one obtains

$$\alpha_m = \Big(\sigma \mathrm{e}^{-\frac{\pi^2 m^2 \sigma^2}{2a^2}} - \xi_m\Big)/|C_m|^2 \quad \text{where} \quad 0 < \xi_m < \varepsilon.$$

On the one hand, truncation of the coefficients α_m at $m = m_0$ such that $\alpha_{m_0} \le \varepsilon$ leads to the bound

$$m_0 \ge \frac{\sqrt{2}}{\pi} \frac{b}{\sigma} \log^{0.5}\left(\frac{\sigma}{(1 + |C_M|^2)\varepsilon}\right) = \frac{\sqrt{2}}{\pi} \frac{b}{\sigma} \log^{0.5}\left(\frac{\sigma}{1 + b}\frac{1}{\varepsilon}\right)$$

for all admissible $\sigma = \sigma_k$. On the other hand, (3.4) implies

$$1/\sigma_k \le c \log(|\log \varepsilon|), \quad k \in \mathcal{T}_l, \quad \text{i.e.,} \quad 1/\sigma_{R_l} \approx \log(|\log \varepsilon|),$$

which ensures the estimate on m_0:

$$m_0 = O(b \log^{3/2}(|\log \varepsilon|)). \tag{3.5}$$

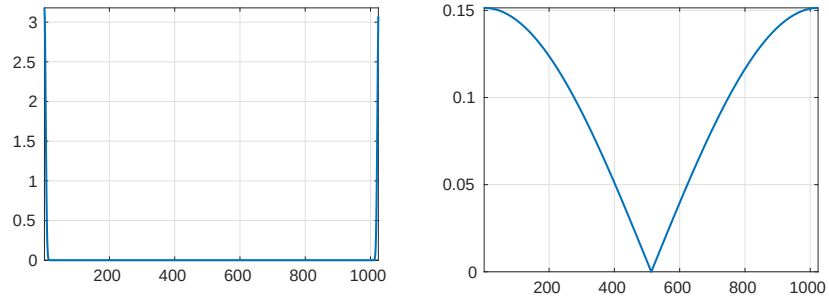

FIG. 5. *Absolute values of the Fourier coefficients of the long-range (left) and short-range (right) discrete Gaussians.*

Now following [32], we represent the Fourier transform of the shifted Gaussians by

$$G_\sigma(x - x_\nu) = \sum_{m=0}^{M} \alpha_m \cos\left(\frac{\pi m(x - x_\nu)}{b}\right) + \eta_\nu, \quad |\eta_\nu| < \varepsilon,$$

which requires only double the number of trigonometric terms compared with the single Gaussian analyzed above. To compensate the possible increase in $|\sum_\nu \eta_\nu|$, we refine $\varepsilon \mapsto \varepsilon/N$. These estimates also apply to all Gaussian functions presented in the long-range sum, since for $k \in \mathcal{T}_l$ they have larger values of σ_k than σ_{R_l}. Indeed, in view of (2.14) the number of summands in the long-range part is of the order $R_l = M/2 = O(\log^2 \varepsilon)$. Combining these arguments with (3.5) proves the resulting estimate. ∎

Figure 5 illustrates fast decay of the absolute values of the Fourier coefficients for the "long-range" discrete Gaussians sampled on an n-point grid (left) with $n = 1024$, and a slow decay of the Fourier coefficients for the "short-range" Gaussians (right). In the latter case, almost all coefficients remain essential, resulting in the full rank decomposition.

To reduce the initial canonical rank NR_l of the low-rank part in the total potential $\mathbf{R}_l$, we apply the multigrid accelerated canonical-to-Tucker (C2T) transform accomplished by the Tucker-to-canonical (T2C) algorithm; see [5]. The complexity of the multigrid C2T transform is of the order of $O(n_m^2 R + r^2 n)$, where $n_m \ll n$ is the starting small grid size, n is the final grid parameter, $R = NR_l$ is the large rank of the initial sum, and r is the maximal Tucker rank. The multigrid acceleration method allows one to avoid the expensive SVD of the complexity $O(R^2 n)$, or $O(Rn^2)$.

Table 1 shows the ranks of sums of long-range ingredients in the electrostatic potentials for the N-particle clusters: the canonical rank NR_N, the rank in the long-range part of the canonical tensor sum NR_ℓ, Tucker ranks $R_{RS,T}$, and the RS canonical rank $R_{RS,C}$ versus the number of particles N and for varying parameters R_ℓ and R_s of the rank-R_N reference canonical tensor. The Newton kernel is generated on the grid with $n^3 = 1024^3$ in the computational box $[-b, b]^3$ with $b = 40$Å, with accuracy $\varepsilon = 10^{-4}$ and canonical rank 21. Particle clusters with 200, 400, and 782 atoms are taken as part of a protein-like multiparticle system. The clusters of size 1728 and 4096 correspond to the lattice structures of size $12 \times 12 \times 12$ and $16 \times 16 \times 16$, respectively, with randomly generated charges. The "RS canonical rank" $R_{RS,C}$ shows the resulting rank after the C2T and T2C transforms with the thresholds $\varepsilon_{C2T} = 4 \cdot 10^{-5}$ and $\varepsilon_{T2C} = 4 \cdot 10^{-6}$. Table 1 demonstrates considerable rank reduction in the canonical

TABLE 1

The tensor ranks of the N-particle potential sum: the initial canonical rank NR_N, the rank of the long-range part in the canonical tensor sum NR_ℓ, Tucker ranks $R_{RS,T}$, and the RS canonical rank $R_{RS,C}$ versus the number of particles N and for varying parameters R_ℓ and R_s of the reference rank-R_N canonical tensor. Grid size $n^3 = 1024^3$.

	N	200	400	782	1728	4096
R_ℓ/R_s	NR	4200	8400	16422	32288	86016
9/12	NR_ℓ	1800	3600	7038	15552	36864
	$R_{RS,T}$	21,16,18	22,19,23	24,22,24	23,24,24	24,24,24
	$R_{RS,C}$	254	292	362	207	243
10/11	NR_ℓ	2000	4000	7820	17280	40960
	$R_{RS,T}$	30,22,25	32,25,33	36,32,34	25,25,25	29,29,29
	$R_{RS,C}$	476	579	768	286	426

TABLE 2

Tucker ranks $R_{RS,T} = (r_1, r_2, r_3)$ for the long-range parts of many-particle potentials versus the number of particles N.

N /R_l	8	9	10	11	12	13
200	10,10,11	13,12,12	18,15,16	23,19,21	32,24,27	42,30,34
400	11,10,11	14,13,14	19,16,20	26,21,26	35,27,36	47,34,47
782	11,11,12	15,14,15	20,18,20	28,26,27	39,35,37	52,46,50

tensor representation and the stable Tucker ranks in the sum of electrostatic potentials when using the range separation approach.

Table 2 displays the Tucker ranks $R_{RS,T} = (r_1, r_2, r_3)$ for the long-range part of the potential sum versus the number of particles N and the chosen long-range part of the reference canonical tensor R_l. The reference Newton kernel is approximated on a 3D grid of size 2048^3, with the rank $R = 29$ and by accuracy $\varepsilon_{\mathcal{N}} = 10^{-5}$. The Tucker tensor is computed using the alternating least squares (ALS) iteration with the stopping criterion $\varepsilon_{T2C} = 10^{-5}$. We observe that for fixed R_l the Tucker ranks $R_{RS,T}$ only moderately increase with respect to the number of particles N. This provides the motivation for introducing the RS tensor format in what follows.

The proof of Theorem 3.1 indicates that the Tucker directional vectors, living on large $n^{\otimes d}$ spatial grids, can be represented in the uniform Fourier basis with a small number of terms. Hence, following the arguments in [21] and [32], we are able to apply the low-rank quantized tensor train (QTT) tensor approximation [36] to these long vectors (see [48] for the case of matrices). The QTT tensor compression allows one to reduce the representation complexity of the long-range part in an RS tensor to the logarithmic scale in the univariate grid size, $O(\log n)$. This will be a topic in a forthcoming paper.

3.2. Quasi-uniformly separable point distributions. The trade-off between the numerical efficiency and approximation quality of the short-range part in the total potential sum can be controlled by introducing the concept of separability of the point set.

DEFINITION 3.2 (Well-separable point distribution). *Given a constant $\sigma_* > 0$, a set $\mathcal{S} = \{x_\nu\}$ of points in $\mathbb{R}^d$ is called σ_*-separable if there holds*

$$d(x_\nu, x_{\nu'}) := \|x_\nu - x_{\nu'}\| \geq \sigma_* \quad \text{for all} \quad \nu \neq \nu'. \tag{3.6}$$

A family of point sets $\{\mathcal{S}_1, \ldots, \mathcal{S}_m\}$ is called uniformly σ_*-separable if (3.6) *holds for every set $\mathcal{S}_{m'}$, $m' = 1, 2, \ldots, m$, independently of the number of particles in a set $\#\mathcal{S}_{m'}$.*

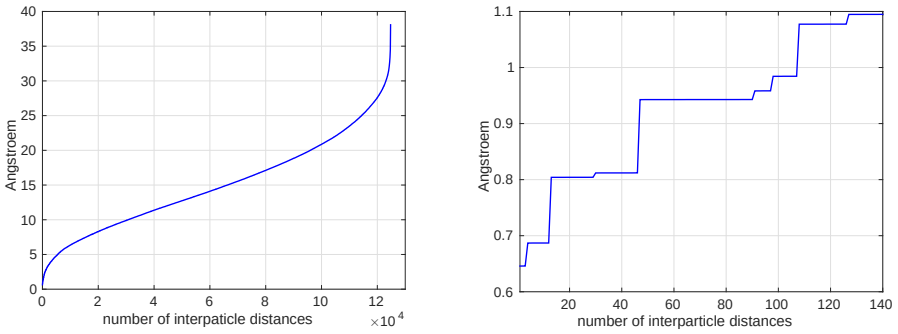

FIG. 6. *Interparticle distances in ascending order for a protein-type structure with* 500 *particles (left). Zoom of the first* 100 *smallest interparticle distances (right).*

Condition (3.6) can be reformulated in terms of the so-called separation distance $q_{\mathcal{S}}$ of the point set $\mathcal{S}$:

$$q_{\mathcal{S}} := \min_{s\in\mathcal{S}} \min_{x_\nu\in\mathcal{S}\setminus s} d(x_\nu, s) \geq \sigma_*. \tag{3.7}$$

Definition 3.2, concerning the separability of point distributions, is fulfilled, particularly in the case of large molecular systems (e.g., proteins, crystals, polymers, nanoclusters), where all atomic centers are strictly separated from each other by a certain fixed *interatomic distance*, e.g., the so-called van der Waals radius. The same happens for lattice-type structures, where each atomic cluster within the unit cell is separated from its neighbors by a distance proportional to the lattice step size. More detailed discussion on the choice of the admissible separation distance $q_{\mathcal{S}}$ is presented in the next section.

The left panel of Figure 6 shows interparticle distances in ascending order for a protein-type structure with $N = 500$ particles. Here and in the following we use the data for a protein-type molecular system provided by the authors of [44]. The total number of distances equals $N(N-1)/2$, where N is the number of particles. The right panel of Figure 6 indicates that the number of particles with small interparticle distances is moderate. In particular, for this example the number of pairs with interparticle distances of less than 1Å is about 0.04 % (≈ 110)) of the total number of $2{,}495{\cdot}10^5$ distances.

Remark 3.3. Notice that for fixed $\sigma > 0$, the σ-separability of the point distributions (see Definition 3.2), which controls the approximation quality of the short-range part, implies that the volume size of the computational box $[-b, b]^3$ should increase proportionally to the number of particles N, i.e., $b = O(N^{1/3})$. Hence, Theorem 3.1 indicates that, since $r_l = O(b)$, the number of entries in the Tucker core of size $r_1 \times r_2 \times r_3$ can be estimated by CN. This asymptotic cost remains of the same order in N as that for the short-range part in the potential sum.

Incorporating periodic boundary conditions is not specifically addressed in this paper. In view of Remark 3.3, we notice that the contribution from the "periodic extension" includes only the long-range component and can be treated in the low-rank tensor format. We refer to section 3.2 of [32] for a discussion of the regularized summation scheme in the periodic setting (see Figures 3.6 and 3.7 in [32]).

3.3. Range-separated canonical and Tucker tensor formats. We recall that the canonical tensor is specified by an R-term sum of rank-1 tensors as in (2.1), hence large values of R complicate operations in this tensor format.[3] In many-particle modeling the initial rank $R = R_0 N$ is proportional to the large number of particles N with a pre-factor of about $R_0 \approx 30$.

The idea on how to get rid of the "curse of ranks," that is, the critical bottleneck in the application of tensor methods to problems such as (3.1), is suggested by results in Theorem 3.1 on the logarithmic bound of the Tucker rank in N for the long-range part in the N-particle potential. The remaining short-range part consists of localized subtensors with nonintersecting supports, each parametrized by the same small-size reference canonical tensor, but differing only in the coordinates of their centers and weights.

Owing to this beneficial property, we introduce the new range-separated (RS) tensor formats based on the aggregated composition of the globally supported low-rank canonical/Tucker tensor, and the set of localized canonical tensors living on the large corporate multi-index set $\mathcal{I} = I_1 \times \cdots \times I_d$.

Such a parametrization attempts to represent the short-range part of a large multidimensional array in $O(N)$ storage (the list of N-particle coordinates) plus the storage of a single small subtensor representing cumulated inclusions. The structure of the *RS canonical/Tucker tensor formats*, specified by a combination of the local-global low-parametric representations, provides good approximation features in the real-space approximation to long-range many-particle interaction potentials.

The following definition introduces cumulated canonical tensors (CCT), describing a sum of short-range potentials with local (up to some threshold) nonintersecting supports.

DEFINITION 3.4 (Cumulated canonical tensors). *Given a set of multi-indices (sources)* $\mathcal{J} = \{\mathbf{j}^{(\nu)} := (j_1^{(\nu)}, j_2^{(\nu)}, \ldots, j_d^{(\nu)})\}$, $\nu = 1, \ldots, N$, $j_\ell^{(\nu)} \in I_\ell$, *and the separation constant* $\sigma_* > 0$, *choose the width parameter* $\gamma \in \mathbb{N}$ *from the relation* $\gamma h \le \sigma_*$ *such that the* γ*-vicinity of each point* $\mathbf{j}^{(\nu)} \in \mathcal{J}$, *i.e.,* $\mathcal{J}_\gamma^{(\nu)} := \{\mathbf{j} : |\mathbf{j} - \mathbf{j}^{(\nu)}| \le \gamma\}$, *does not intersect all others:*

$$\mathcal{J}_\gamma^{(\nu)} \cap \mathcal{J}_\gamma^{(\nu')} = \varnothing, \quad \nu \ne \nu'.$$

A rank-R_0 *CCT tensor* $\widehat{\mathbf{U}} \in \mathbb{R}^{\mathcal{I}}$, *associated with* $\mathcal{J}$ *and the width parameter* γ, *is defined as a set of tensors which can be represented in the form*

$$\widehat{\mathbf{U}} = \sum\nolimits_{\nu=1}^{N} c_\nu \mathbf{U}_\nu \quad \textit{with} \quad \operatorname{rank}(\mathbf{U}_\nu) \le R_0, \tag{3.8}$$

where canonical tensors $\mathbf{U}_\nu = [u_{\mathbf{j}}]$ *are vanishing beyond the* γ*-vicinity of* $\mathbf{j}^{(\nu)}$*:*

$$u_{\mathbf{j}} = 0 \quad \textit{for} \quad \mathbf{j} \subset \mathcal{I} \setminus \mathcal{J}_\gamma^{(\nu)}, \quad \nu = 1, \ldots, N. \tag{3.9}$$

Given the particular point set $\mathcal{S}$, the effective support of the localized subtensors should be of a size close to the parameter $\sigma_* > 0$, appearing in Definition 3.2, that introduces the σ_*-separable point distributions characterized by the separation parameter $\sigma_* > 0$. In this case, we use the relation $\sigma_* \approx \gamma h$, where $h = 2b/n$ is the mesh size of the computational $(n \times \cdots \times n)$-grid.

[3] Notice that the subclass of the so-called *orthogonal canonical tensors* [40] allows stable rank reduction, but suffers from poor approximation capacity. Another class of "monotone" tensors providing stable canonical representation is specified by all positive canonical vectors (see [39, 34] for a definition), which is the case in the decomposition of the elliptic Green's kernels. Both classes of tensors do not suit problems such as (3.1).

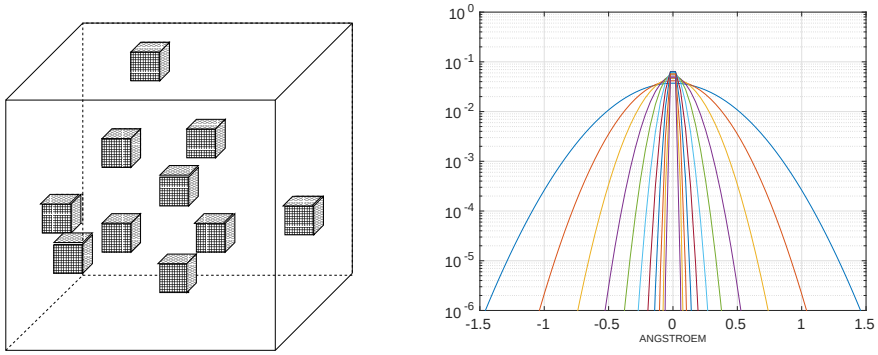

FIG. 7. *Schematic illustration of effective supports of the CCT (left). Short-range canonical vectors for $k = 1, \dots, 11$, presented in the logarithmic scale (right).*

The left panel of Figure 7 illustrates the effective supports of a CCT in the nonoverlapping case, while the right panel presents the supports for the first 11 short-range canonical vectors (selected from rank-24 reference canonical tensor $\mathbf{P}_R$), which allows the choice of the parameter γ in the separation criteria.

The CCTs have beneficial features which are particularly useful in the low-rank tensor approximation of many-particle interaction potentials.

PROPOSITION 3.5 (Properties of CCT). (A) *The local rank of a CCT tensor* $\widehat{\mathbf{U}}$ *is bounded by* R_0*:*

$$\mathrm{rank}_{loc}(\widehat{\mathbf{U}}) := \max_{\nu} \mathrm{rank}(\mathbf{U}_\nu) \le R_0.$$

(B) *Local components in the CCT* (3.8) *are "block orthogonal" in the sense of*

$$\langle \mathbf{U}_\nu, \mathbf{U}_{\nu'} \rangle = 0 \quad \forall \nu \neq \nu'. \tag{3.10}$$

(C) *There holds* $\|\widehat{\mathbf{U}}\|^2 = \sum_{\nu=1}^{N} c_\nu^2 \|\mathbf{U}_\nu\|^2$.

Proof. Properties (A) and (B) simply follow by definition of the CCT, while (C) is a direct consequence of (B). ∎

If $R_0 = 1$, i.e., $\widehat{\mathbf{U}}$ is the usual rank-N canonical tensor, then property (B) in Proposition 3.5 leads to the definition of orthogonal canonical tensors in [40]; hence, in the case $R_0 > 1$, we arrive at the generalization further called the *block orthogonal canonical tensors*.

The separation criteria in Definition 3.4 lead to a rather "aggressive" strategy for selecting the short-range part $\mathbf{P}_{R_s}$ in the reference canonical tensor $\mathbf{P}_R$ at the benefit of easy implementation of the CCT (nonoverlapping case). However, in some cases this may lead to overestimation of the Tucker/canonical rank in the long-range tensor component. To relax the criteria in Definition 3.4, we propose a "soft" strategy that allows us to include a few (i.e., $O(1)$ for large N) neighboring particles into the local vicinity $\mathcal{J}_\gamma^{(\nu)}$ of the source point x_ν, which can be achieved by increasing the overlap parameter $\gamma > 0$. This allows us to control both the bound on the rank parameter of the long-range tensor almost uniformly in N and the complexity of the CCT tensors $\widehat{\mathbf{U}}$.

Remark 3.6. Our strategy for splitting of the reference potential into short- and long-range parts is based on the control of the overlap region for the short-range part compared with the typical "interparticle distance" in the considered system of quasi-uniformly distributed particles. The principal difference of our approach from

the existing Ewald summation schemes is the rank-structured representation of both short- and long-range parts in the reference kernel, which allows one to split the difficulties and then efficiently perform the summation of both localized and global parts in the total potential sum by using different tensor formats. However, the traditional generating kernels may depend on parameters whose variation could significantly alter their "effective support," so that the balance (correlation) between the short- and long-range components may vary dramatically. In such a scenario the adaptive RS splitting can be useful for rather general classes of generating kernels.

Example 1. Assume that the separation distance is equal to $\sigma_* = 0.8$Å, corresponding to the example in the right panel of Figure 6, and the computational threshold is given as $\varepsilon = 10^{-4}$. Then we find from the right panel of Figure 7 that the "aggressive" criteria in Definition 3.4 lead to the choice $R_s = 10$, since the value of the canonical vector with $k = 11$ at the point $x = \sigma_*$ is about 10^{-3}. Hence, in order to control the required rank parameter R_l, we have to extend the overlap area to the larger parameter σ_* and, hence, to larger γ. This will lead to a small $O(1)$-overlap between the supports of the short-range tensor components, but without asymptotic increase in the total complexity.

In the following, we distinguish a special subclass of *uniform CCTs*.

DEFINITION 3.7 (Uniform CCTs). *A CCT tensor in* (3.8) *is called uniform if all components* $\mathbf{U}_\nu$ *are generated by a single rank-*R_0 *tensor* $\mathbf{U}_0 = \sum_{m=1}^{R_0} \mu_m \hat{\mathbf{u}}_m^{(1)} \otimes \cdots \otimes \hat{\mathbf{u}}_m^{(d)}$ *such that* $\mathbf{U}_\nu|_{\mathcal{J}_\delta^{(\nu)}} = \mathbf{U}_0$.

Now we are in a position to define the RS canonical and Tucker tensor formats in $\mathbb{R}^{n_1 \times \cdots \times n_d}$.

DEFINITION 3.8 (RS canonical tensors). *Given the separation parameter* $\gamma \in \mathbb{N}$, *the RS canonical tensor format specifies the class of* d*-tensors* $\mathbf{A} \in \mathbb{R}^{n_1 \times \cdots \times n_d}$ *which can be represented as the sum of a rank-*R *canonical tensor* $\mathbf{U} = \sum_{k=1}^{R} \xi_k \mathbf{u}_k^{(1)} \otimes \cdots \otimes \mathbf{u}_k^{(d)} \in \mathbb{R}^{n_1 \times \cdots \times n_d}$ *and a (uniform) CCT tensors* $\widehat{\mathbf{U}} = \sum_{\nu=1}^{N} c_\nu \mathbf{U}_\nu$ *generated by* $\mathbf{U}_0$ *with* $\mathrm{rank}(\mathbf{U}_0) \le R_0$ *as in Definition* 3.7 *(or more generally in Definition* 3.4*):*

$$\mathbf{A} = \sum\nolimits_{k=1}^{R} \xi_k \mathbf{u}_k^{(1)} \otimes \cdots \otimes \mathbf{u}_k^{(d)} + \sum\nolimits_{\nu=1}^{N} c_\nu \mathbf{U}_\nu, \tag{3.11}$$

where $\mathrm{diam}(\mathrm{supp}\mathbf{U}_\nu) \le 2\gamma$ *in the index size.*

For a given $\mathbf{A}$ and a grid point $\mathbf{i} \in \mathcal{I} = I_1 \times \cdots \times I_d$, we define the set of indexes

$$\mathcal{L}(\mathbf{i}) := \{\nu \in \{1, \ldots, N\} : \mathbf{i} \in \mathrm{supp}\mathbf{U}_\nu\},$$

labeling all short-range tensors $\mathbf{U}_\nu$, which include the grid point $\mathbf{i}$ within their effective support.

LEMMA 3.9. *The storage cost of the RS canonical tensor* $\mathbf{A}$ *in* (3.11) *is estimated by*

$$\mathrm{stor}(\mathbf{A}) \le dRn + (d+1)N + dR_0\gamma.$$

Given $\mathbf{i} \in \mathcal{I}$, *denote by* $\overline{\mathbf{u}}_{i_\ell}^{(\ell)} \in \mathbb{R}^{1 \times R}$ *the row vector with index* i_ℓ *in the side matrix* $U^{(\ell)} \in \mathbb{R}^{n_\ell \times R}$ *of* $\mathbf{U}$, *and let* $\xi = (\xi_1, \ldots, \xi_d)$. *Then the* $\mathbf{i}$*th entry of the RS canonical tensor* $\mathbf{A} = [a_{\mathbf{i}}]$ *can be calculated as a sum of long- and short-range contributions by*

$$a_{\mathbf{i}} = \left(\odot_{\ell=1}^{d} \overline{\mathbf{u}}_{i_\ell}^{(\ell)} \right) \xi^T + \sum_{\nu \in \mathcal{L}(\mathbf{i})} c_\nu \mathbf{U}_\nu(\mathbf{i})$$

at the expense $O(dR + 2d\gamma R_0)$.

Proof. Definition 3.8 implies that each RS canonical tensor is uniquely defined by the following parametrization: the rank-R canonical tensor $\mathbf{U}$, the rank-R_0 local reference canonical tensor $\mathbf{U}_0$ with the mode size bounded by 2γ, and a list $\mathcal{J}$ of the coordinates and weights of the N particles. Hence the storage cost directly follows. To justify the entrywise representation complexity, we notice that by the well-separability assumption (see Definition 3.2) we have $\#\mathcal{L}(\mathbf{i}) = O(1)$ for all $\mathbf{i} \in \mathcal{I}$. This proves the complexity bound. ∎

Now we define the class of RS Tucker tensors.

DEFINITION 3.10 (RS Tucker tensors). *Given the separation parameter $\gamma \in \mathbb{N}$, the RS Tucker tensor format specifies the class of d-tensors $\mathbf{A} \in \mathbb{R}^{n_1 \times \cdots \times n_d}$, which can be represented as the sum of a rank-$\mathbf{r}$ Tucker tensor $\mathbf{V}$ and a (uniform) CCT generated by $\mathbf{U}_0$ with* $\mathrm{rank}(\mathbf{U}_0) \le R_0$ *as in Definition* 3.7 *(or more generally in Definition* 3.4*):*

$$\mathbf{A} = \boldsymbol{\beta} \times_1 V^{(1)} \times_2 V^{(2)} \cdots \times_d V^{(d)} + \sum\nolimits_{\nu=1}^{N} c_\nu \mathbf{U}_\nu, \tag{3.12}$$

where the tensor $\mathbf{U}_\nu$, $\nu = 1, \ldots, N$, has local support, i.e., $\mathrm{diam}(\mathrm{supp}\mathbf{U}_\nu) \le 2\gamma$.

Similarly to Lemma 3.9, the complexity bounds for the RS Tucker tensors can be proven.

LEMMA 3.11. *The storage size for the RS Tucker tensor does not exceed*

$$\mathrm{stor}(\mathbf{A}) \le r^d + drn + (d+1)N + dR_0\gamma.$$

Let the r_ℓ-vector $\mathbf{v}_{i_\ell}^{(\ell)} \in \mathbb{R}^{1 \times r_\ell}$ be the i_ℓ row of the matrix $V^{(\ell)} \in \mathbb{R}^{n_\ell \times r_\ell}$. Then the $\mathbf{i}$th element of the tensor $\mathbf{A} = [a_\mathbf{i}]$ can be calculated at the expense $O(r^d + 2d\gamma R_0)$ by

$$a_\mathbf{i} = \boldsymbol{\beta} \times_1 \mathbf{v}_{i_1 l}^{(1)} \times_2 \mathbf{v}_{i_2}^{(2)} \cdots \times_d \mathbf{v}_{i_d}^{(d)} + \sum_{\nu \in \mathcal{L}(\mathbf{i})} c_\nu \mathbf{U}_\nu(\mathbf{i}). \tag{3.13}$$

Proof. In view of Definition 3.10, the RS Tucker tensor is uniquely defined by the following parametrization: the rank-$\mathbf{r} = (r_1, \ldots, r_d)$ Tucker tensor $\mathbf{V} \in \mathbb{R}^{n_1 \times \cdots \times n_d}$, the rank-$R_0$ local reference canonical tensor $\mathbf{U}_0$ with $\mathrm{diam}(\mathrm{supp}\mathbf{U}_0) \le 2\gamma$, and a list $\mathcal{J}$ of the coordinates of the N particle centers $\{x_\nu\}$ and N weights $\{c_\nu\}$. This proves the storage complexity. The entrywise representation complexity follows by (3.13). ∎

The main computational benefits of the new RS canonical/Tucker tensor formats are demonstrated by the uniform bounds on the Tucker rank of the long-range part in the large sum of interaction potentials (see Theorem 3.1 and the numerics in section 3.1). Moreover, we have the low storage cost for the RS canonical/Tucker tensors, cheap representation of each entry in an RS tensor, and the possibility for simple implementation of multilinear algebra on these tensors (see section 3.4), which opens the opportunities for various applications.

Figure 8 displays the accuracy of the RS tensor approximation to the electrostatic potential of a cluster with 500 particles at the middle section of the computational box $[-20, 20]^3$ Å by using an $n \times n \times n$ 3D Cartesian grid with $n = 1024$ and step size $h = 0.04$Å. The top-left figure shows the surface of the potential at the level $z = 0$, while the top-right figure shows the absolute error of the RS approximation with $R_l = 15$, $R_s = 11$, and $\sigma^* = 1.5$. The bottom figures visualize the long-range (left) and short-range (right) parts of the RS tensor, representing the potential sum.

The most time-consuming part in our scheme is the canonical-to-Tucker algorithm for computing the long-range part of the RS format tensors. Table 3 indicates almost

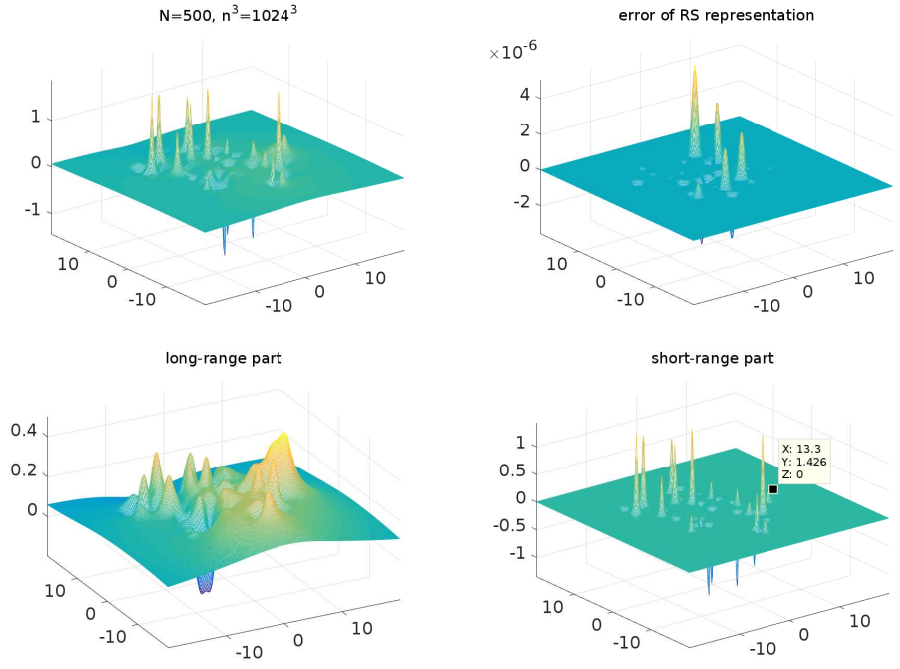

FIG. 8. *Top: the sum of electrostatic potentials at the middle plane of a cluster with* 500 *particles (left), and the error of its RS approximation (right). Bottom: long-range part of a sum (left); short-range part of a sum (right).*

TABLE 3

Times (sec) for a canonical-to-Tucker rank reduction versus number of particles N and grid size n^3.

N /n^3	512^3	1024^3	2048^3	4096^3	8192^3	16384^3	$R_{RS,C}$
100	0.9	1.5	2.3	4.1	6.0	12.2	183
200	2.3	3.0	4.7	7.9	14.4	23.4	214
400	5.2	7.0	8.7	16.1	32.9	71.7	227
770	12.3	13.8	18.3	32.7	67.5	147.3	290

linear scaling in the number of particles and in the univariate grid size n of the $n\times n\times n$ representation grid. The rightmost column shows the resulting canonical ranks $R_{RS,C}$ of the side matrices $U^{(\ell)}$, $\ell = 1,\ 2,\ 3$ in (3.11). The asymptotically optimal complexity scaling of the RS decomposition and the required storage provides the main motivation for further applications of the RS tensor format.

Remark 3.12. It is worth noting that in the case of higher dimensions, say, for $d > 3$, the local canonical tensors can be combined with the global tensor train (TT) format [49] such that the simple canonical-to-TT transform can be applied. This introduces the RS-TT format as a set of tensors represented by a sum of CCT terms and the global low-rank TT tensor. The complexity and structural analysis is very similar to the case of RS canonical and RS Tucker formats.

3.4. Algebraic operations on the RS canonical/Tucker tensors. Multilinear algebraic operations in the format of RS canonical/Tucker tensor parametrization can be implemented by using 1D vector operations applied to both localized and global

tensor components. In particular, the following operations on RS canonical/Tucker tensors can be realized efficiently: (a) storage of a tensor; (b) real-space representation on a fine rectangular grid; (c) summation of many-particle interaction potentials represented on the fine tensor grid; and (d) computation of scalar products.

Estimates on the storage complexity for the RS canonical and RS Tucker formats are presented in Lemmas 3.9 and 3.11. Items (b) and (c) have already been addressed in the previous part. Calculation of the scalar product of two RS canonical tensors in the form (3.11), defined on the same set $\mathcal{S}$ of particle centers, can be reduced to the standard calculation of the cross-scalar products between all elementary canonical tensors presented in (3.11). The numerical cost is bounded by $O(\frac{1}{2}R(R-1)dn + 2\gamma RR_0N)$.

4. Applications of the RS format in data modeling and in many-particle calculations. The RS tensor formats can be gainfully applied in computational problems involving functions with multiple local singularities or cusps, as well as Green's kernels with essentially nonlocal behavior; they can also be applied in multidimensional approximation problems treated by means of radial basis functions. In [5], the RS approach was applied to computation of gradients and forces for many-particle interaction potentials, and to the construction of approximate boundary/interface conditions in the Poisson–Boltzmann equation describing the electrostatic potential of proteins.

In what follows, we discuss how the RS tensor representations can be utilized in computationally extensive problems related to the grid representation of multidimensional scattered data, and for computation of the interaction energy of a charged many-particle system.

4.1. Multidimensional data modeling. In this section, we briefly describe the model reduction approach to the problem of multidimensional data fitting based on the RS tensor approximation. The problems of multidimensional scattered data modeling and data mining are known to lead to computationally intensive simulations. We refer to [12, 31, 9, 23, 28] for discussion of the most commonly used computational approaches in this field of numerical analysis.

The mathematical problems in scattered data modeling are concerned with the approximation of the multivariate function $f : \mathbb{R}^d \to \mathbb{R}$ ($d \geq 2$) by using samples given at a certain finite set $\mathcal{X} = \{x_1, \ldots, x_N\} \subset \mathbb{R}^d$ of pairwise distinct points; see, e.g., [12]. The function f may describe the surface of a solid body, the solution of a PDE, a many-body potential field, the multiparametric characteristics of physical systems, or some other multidimensional data.

In the particular problem setting one may be interested in recovering f from a given sampling vector $f_{|\mathcal{X}} = (f(x_1), \ldots, f(x_N)) \in \mathbb{R}^N$. One of the traditional ways to tackle this problem is based on the construction of a suitable functional interpolant $P_N : \mathbb{R}^d \to \mathbb{R}$ satisfying $P_{N|\mathcal{X}} = f_{|\mathcal{X}} =: \mathbf{f}$, i.e.,

$$P_N(x_j) = f(x_j) \quad \forall\, 1 \leq j \leq N, \tag{4.1}$$

or approximating the sampling vector $f_{|\mathcal{X}}$ on the set $\mathcal{X}$ in the least-squares sense. We consider the approach based on the use of *radial basis functions*, which provide the traditional tools for multivariate scattered data interpolation. To that end, the radial basis function (RBF) interpolation approach deals with a class of interpolants P_N in the form

$$P_N(x) = \sum_{j=1}^{N} c_j p(\|x - x_j\|) + Q(x), \quad Q \text{ is some smooth function}, \tag{4.2}$$

where $p : [0, \infty) \to \mathbb{R}$ is a fixed radial function and $\|\cdot\|$ is the Euclidean norm on $\mathbb{R}^d$. To fix the idea, here we consider the particular version of (4.2) by setting $Q = 0$. Notice that the interpolation ansatz P_N in (4.2) has the same form as the multiparticle interaction potential in (3.1). This observation indicates that the numerical treatment of various problems based on the use of the interpolant P_N can be handled by using the same tools of model reduction via rank-structured RS tensor approximation.

The particular choice of RBFs described in [12, 31] includes functions $p(r)$ in the form

$$r^\nu, \quad (1 + r^2)^\nu, \ (\nu \in \mathbb{R}), \quad \exp(-r^2), \quad r^2 \log(r),$$

where $r = \|x\|$. For our tensor-based approach, the common feature of all these function classes is the existence of low-rank tensor approximations to the grid-based discretization of the RBF $p(\|x\|) = p(x_1, \ldots, x_d)$, $x \in \mathbb{R}^d$. We can extend the above examples with traditional functions commonly used in quantum chemistry, such as the Coulomb potential $1/r$, the Slater function $\exp(-\lambda r)$, and the Yukawa potential $\exp(-\lambda r)/r$, as well as the class of Matérn RBFs traditionally applied in stochastic modeling [47]. Other examples are given by the Lennard-Jones (Van der Waals) $p(r) = 4\epsilon[(\frac{\sigma}{r})^{12} - (\frac{\sigma}{r})^6]$ and dipole-dipole interaction potentials $p(r) = \frac{1}{r^3}$, as well as the Stokeslet [45], specified by the 3×3 matrix $p(\|x\|) = I/r + (xx^T)/r^3$ for $x \in \mathbb{R}^3$.

In the context of numerical data modeling, we focus on the following computational tasks.

(A) For a fixed coefficient vector $\mathbf{c} = (c_1, \ldots, c_N)^T \in \mathbb{R}^N$, find the efficient representation and storage of the interpolant in (4.2), sampled on a fine tensor grid in $\Omega \subset \mathbb{R}^d$, that allows the $O(1)$-fast point evaluation of P_N in the whole volume Ω and computation of various integro-differential operations on that interpolant, such as gradients, forces, scalar products, convolution integrals, etc.

(B) Find the coefficient vector $\mathbf{c}$ that solves the interpolation problem (4.1).

We approach problems (A) and (B) with the intent to apply the RS tensor representation to the interpolant $P_N(x)$. The point is that representation (4.2) can be viewed as the many-particle interaction potential (with charges c_j) considered in the previous sections. Hence, the RS tensor approximation can be successfully applied if the d-dimensional tensor approximating the RBF $p(\|x\|)$, $x \in \mathbb{R}^d$, on the tensor grid allows a low-rank canonical representation that can be split into short- and long-range parts. This can be proven for the functions listed above (see the example in section 2.2 for the Newton kernel $1/\|x\|$). Notice that the Gaussian is already the rank-1 separable function.

Problem (A). To fix the idea, we consider the particular choice of the set $\mathcal{X} \subset \Omega := [0, 1]^d$, which can be represented by using almost optimal point sampling. The so-called optimal point sets realize the trade-off between the separation distance $q_{\mathcal{X}} = \min_{s \in \mathcal{X}} \min_{x_\nu \in \mathcal{X} \setminus s} d(x_\nu, s)$ (see (3.7)) and the fill distance $h_{\mathcal{X},\Omega} = \max_{y \in \Omega} d(\mathcal{X}, y)$, i.e., they solve the problem (see [12])

$$q_{\mathcal{X}}/h_{\mathcal{X},\Omega} \to \max.$$

We choose the set of points $\mathcal{X}$ as a subset of the $n^\otimes$ square grid Ω_h with the mesh size $h = 1/(n-1)$ such that the separation distance satisfies $\sigma_* = q_{\mathcal{X}} \geq \alpha h$, $\alpha \geq 1$. Here $N \leq n^d$. The square grid Ω_h realizes an example of the almost optimal point

set (see the discussion in [31]). The construction below also applies to nonuniform rectangular grids.

Now we are in a position to apply the RS tensor representation to the total interpolant P_N. Let $\mathbf{P}_R$ be the $n \times n \times n$ (say, for $d = 3$) rank-R tensor representing the RBF $p(\|\cdot\|)$ which allows RS splitting by (2.11), generating the global RS representation (3.2). Then $P_N(x)$ can be represented by the tensor $\mathbf{P}_N$ in the RS Tucker (3.12) or RS canonical (3.11) formats. The storage cost scales linearly in both N and n, $O(N + dR_l n)$. The tensor-based computation of different functionals on $\mathbf{P}_N$ will be discussed in the following sections.

Problem (B). The interpolation problem (4.1) reduces to solve the linear system of equations for an unknown coefficient vector $\mathbf{c} = (c_1, \dots, c_N)^T \in \mathbb{R}^N$,

$$A_{p,\mathcal{X}}\mathbf{c} = \mathbf{f}, \quad \text{where} \quad A_{p,\mathcal{X}} = [p(\|x_i - x_j\|)]_{1\le i,j\le N} \in \mathbb{R}^{N\times N} \tag{4.3}$$

with the symmetric matrix $A_{p,\mathcal{X}}$ (in some applications it is called the covariance matrix). Here, without loss of generality, we assume that the RBF, $p(\|\cdot\|)$, is continuous. The solvability conditions for the linear system (4.3) with the matrix $A_{p,\mathcal{X}}$ are discussed, for example, in [12]. We consider two principal cases.

Case (A). We assume that the point set $\mathcal{X}$ coincides with the set of grid points in Ω_h, i.e., $N = n^d$. Introducing the d-tuple multi-index $\mathbf{i} = (i_1, \dots, i_d)$ and $\mathbf{j} = (j_1, \dots, j_d)$, we reshape the matrix $A_{p,\mathcal{X}}$ into the tensor form

$$A_{p,\mathcal{X}} \mapsto \mathbf{A} = [a(i_1, j_1, \dots, i_d, j_d)] \in \bigotimes_{\ell=1}^{d} \mathbb{R}^{n\times n},$$

which corresponds to the folding of an N-vector to a d-dimensional $n^{\otimes d}$ tensor. This d-level Toeplitz matrix is generated by the tensor $\mathbf{P}_R$ obtained by collocation of the RBF $p(\|\cdot\|)$ on the grid Ω_h. Splitting the rank-R canonical tensor $\mathbf{P}_R$ into a sum of short- and long-range terms,

$$\mathbf{P}_R = \mathbf{P}_{R_s} + \mathbf{P}_{R_l} \quad \text{with} \quad \mathbf{P}_{R_l} = \sum_{k=1}^{R_l} \mathbf{p}_k^{(1)} \otimes \cdots \otimes \mathbf{p}_k^{(d)},$$

allows us to represent the matrix $\mathbf{A}$ in the RS canonical form as a sum of low-rank canonical tensors $\mathbf{A} = \mathbf{A}_{R_s} + \mathbf{A}_{R_l}$. Here, the first one corresponds to the diagonal (or almost diagonal in the case of the "soft" separation strategy) matrix by assumption on the locality of $\mathbf{P}_{R_s}$. The second matrix takes the form of the R_l-term Kronecker product sum

$$\mathbf{A}_{R_l} = \sum\nolimits_{k=1}^{R_l} A_k^{(1)} \otimes \cdots \otimes A_k^{(d)},$$

where each "univariate" matrix $A_k^{(\ell)} \in \mathbb{R}^{n\times n}$, $\ell = 1, \dots, d$, takes the symmetric Toeplitz form generated by the first column vector $\mathbf{p}_k^{(\ell)}$. The storage complexity of the resultant RS representation to the matrix $\mathbf{A}$ is estimated by $O(N+dR_l n)$. Similar matrix decompositions can be derived for the RS Tucker and RS-TT representations of $\mathbf{P}_R$.

Now we represent the coefficient vector $\mathbf{c} \in \mathbb{R}^N$ as the d-dimensional $n^{\otimes d}$ tensor $\mathbf{c} \mapsto \mathbf{C} \in \mathbb{R}^{n^{\otimes d}}$. Then the matrix-vector multiplication $\mathbf{AC} = (\mathbf{A}_{R_s} + \mathbf{A}_{R_l})\mathbf{C}$ implemented in tensor format can be accomplished in $O(cN + dR_l N \log n)$ operations, i.e., with the asymptotically optimal cost in the number of sampling points N. The

reason is that the matrix $\mathbf{A}_{R_s}$ has the diagonal form, while the matrix-vector product between the Toeplitz matrices $A_k^{(\ell)}$ constituting the Kronecker factors $\mathbf{A}_{R_l}$ and the corresponding n-columns (fibers) of the tensor $\mathbf{C}$ can be implemented by 1D FFT in $O(n \log n)$ operations. One can enhance this scheme by introducing the low-rank tensor structure in the target vector (tensor) $\mathbf{C}$.

Case (B). This construction can be generalized to the situation where $\mathcal{X}$ is a subset of Ω_h, i.e., $N < n^d$. In this case the complexity again scales linearly in N if $N = O(n^d)$. In the situation where $N \ll n^d$, the matrix-vector operation applies to the vector $\mathbf{C}$ that vanishes beyond the small set $\mathcal{X}$. In this case the corresponding block-diagonal submatrices in $A_k^{(\ell)}$ lose the Toeplitz form, thus resulting in a slight increase in the overall cost $O(N^{1+1/d})$.

In both cases (A) and (B), the presented new construction can be applied within any favorable preconditioned iteration for solving the linear system (4.3).

4.2. Interaction energy for a charged many-particle system. Consider the calculation of the interaction energy for a charged multiparticle system. In the case of lattice-structured systems, the fast tensor-based computation scheme for the interaction energy was described in [33]. Recall that the interaction energy of the total electrostatic potential generated by the system of N charged particles located at $x_k \in \mathbb{R}^3$ $(k = 1, \dots, N)$ is defined by the weighted sum

$$E_N = E_N(x_1, \dots, x_N) = \frac{1}{2} \sum_{j=1}^{N} z_j \sum_{k=1, k \neq j}^{N} \frac{z_k}{\|x_j - x_k\|}, \tag{4.4}$$

where z_k denotes the particle charge. Letting $\sigma > 0$ be the minimal physical distance between the centers of particles, we arrive at the σ-separable systems in the sense of Definition 3.2. The double sum in (4.4) applies only to the particle positions $\|x_j - x_k\| \geq \sigma$, hence the quantity in (4.4) is computable also for singular kernels such as $p(r) = 1/r$.

We observe that the quantity of interest E_N can be recast in terms of the interconnection matrix $A_{p,\mathcal{X}}$ defined by (4.3) with $p(r) = 1/r$, $\mathcal{X} = \{x_1, \dots, x_N\}$:

$$E_N = \frac{1}{2} \langle (A_{p,\mathcal{X}} - \mathrm{diag} A_{p,\mathcal{X}}) \mathbf{z}, \mathbf{z} \rangle, \quad \text{where} \quad \mathbf{z} = (z_1, \dots, z_N)^T. \tag{4.5}$$

Hence, E_N can be calculated by using the approach briefly addressed in the previous section.

We now describe this scheme in more detail. Recall that the reference canonical tensor $\mathbf{P}_R$ approximating the single Newton kernel on an $n \times n \times n$ tensor grid Ω_h in the computational box $\Omega = [-b, b]^3$ is represented by (2.9), where $h > 0$ is the fine mesh size. For ease of exposition, we assume that the particle centers x_k are located exactly at some grid points in Ω_h (otherwise, an additional approximation error may be introduced) such that each point x_k inherits some multi-index $\mathbf{i}_k \in \mathcal{I}$, and the origin $x = 0$ corresponds to the central point on the grid, $\mathbf{n}_0 = (n/2, n/2, n/2)$. In turn, the canonical tensor $\mathbf{P}_0$ approximating the total interaction potential $P_N(x)$ $(x \in \Omega)$ for the N-particle system

$$P_N(x) = \sum_{k=1}^{N} \frac{z_k}{\|x - x_k\|} \rightsquigarrow \mathbf{P}_0 = \mathbf{P}_s + \mathbf{P}_l \in \mathbb{R}^{n \times n \times n}$$

is represented by (3.2) as the sum of short- and long-range tensor components. Now the tensor $\mathbf{P}_0 = \mathbf{P}_0(x^h)$ is defined at each point $x^h \in \Omega_h$, and, in particular, in the

vicinity of each particle center x_k, i.e., at the grid points $x_k+h\mathbf{e}$, where the directional vector $\mathbf{e} = (e_1, e_2, e_3)^T$ is specified by some choice of coordinates $e_\ell \in \{-1, 0, 1\}$ for $\ell = 1, 2, 3$. This allows us to introduce the useful notation $\mathbf{P}_0(x_k + h\mathbf{e})$, which can be applied to all tensors living on Ω_h. Such notation simplifies the definitions of entities such as energy, gradients, forces, etc. applied to the RS tensors.

Remark 4.1. The assumption that particle coordinates are placed exactly at grid points in Ω_h often arises in many-particle computations. In particular, the meshing-up step is present in most Ewald summation methods, where the spatial resolution (accuracy) is limited by the total size of the 3D grid in the volume, and by the respective 3D FFT. Our tensor approach scales linearly (not cubically) in the univariate grid size hence we have facilities for the fine spatial resolution of the potential (say, on $10^4 \times 10^4 \times 10^4$ grids), meaning minor limitations on the grid size. Moreover, the calculation of the interaction energy and forces can basically be performed in terms of the smooth long-range part in the total potential which allows good resolution on the grid, depending weakly on small perturbations in the centers of charges.

The following lemma describes the tensor-based scheme for calculating the approximation $E_{N,T}$ to E_N by utilizing the long-range part $\mathbf{P}_l$ only in the tensor representation of $P_N(x)$.

LEMMA 4.2. *Let the effective support of the short-range components in the reference potential $\mathbf{P}_R$ not exceed $\sigma > 0$. Then the interaction energy E_N of the N-particle system can be calculated by using only the long-range part in the total potential sum*

$$E_{N,T} = E_{N,RS}(x_1, \dots, x_N) = \frac{1}{2} \sum_{j=1}^{N} z_j (\mathbf{P}_l(x_j) - z_j \mathbf{P}_{R_l}(x = 0)) \tag{4.6}$$

in $O(dR_lN)$ operations, where R_l is the canonical rank of the long-range component.

Proof. Similarly to [33], where the case of lattice-structured systems was analyzed, we show that the interior sum in (4.4) can be obtained from the tensor $\mathbf{P}_0$ traced onto the centers of particles x_k, where the term corresponding to $x_j = x_k$ is removed:

$$\sum_{k=1, k\neq j}^{N} \frac{z_k}{\|x_j - x_k\|} \rightsquigarrow \mathbf{P}_0(x_j) - z_j \mathbf{P}_R(x = 0).$$

Here the value of the reference canonical tensor $\mathbf{P}_R$ (see (2.9)) is evaluated at the origin $x = 0$, i.e., corresponding to the multi-index $\mathbf{n}_0 = (n/2, n/2, n/2)$. Hence, we arrive at the tensor approximation

$$E_{N,T} \rightsquigarrow \frac{1}{2} \sum_{j=1}^{N} z_j (\mathbf{P}_0(x_j) - z_j \mathbf{P}_R(x = 0)). \tag{4.7}$$

Now we split $\mathbf{P}_0$ into the long-range part (3.3) and the remaining short-range potential to obtain $\mathbf{P}_0(x_j) = \mathbf{P}_s(x_j) + \mathbf{P}_l(x_j)$; we then do the same for the reference tensor $\mathbf{P}_R$. By assumption, the short-range part $\mathbf{P}_s(x_j)$ at point x_j in (4.7) consists only of the local term $P_{R_s}(x = 0) = z_j \mathbf{P}_R(x = 0)$. Due to the corresponding cancellations in the right-hand side of (4.7), we find that E_N depends only on $\mathbf{P}_l$, leading to the final tensor representation in (4.6).

We arrive at the linear complexity scaling $O(dR_lN)$, taking into account the $O(dR_l)$ cost of the point evaluation for the canonical tensor $\mathbf{P}_l$. ∎

TABLE 4

Accuracy of the tensor approximation $E_{N,T}$ to the interaction energy of an N-particle cluster E_N by using a full canonical tensor representation of the cluster potential ($R_s = 0$).

grid size	N	100	200	400	782
	E_N	-8.4888	-18.1712	-35.9625	-90.2027
8192^3	er_T	0.0028	0.005	0.0074	0.0245
	$er_{T,rel}$	$3 \cdot 10^{-4}$	$3 \cdot 10^{-4}$	$2 \cdot 10^{-4}$	$3 \cdot 10^{-4}$
16384^3	er_T	0.0021	0.0013	0.0039	0.0053
	$er_{T,rel}$	$2 \cdot 10^{-4}$	10^{-4}	10^{-4}	10^{-4}

TABLE 5

Accuracy of the tensor approximation $E_{N,T}$ to the interaction energy of an N-particle cluster E_N when using the RS tensor approximation with $R_l = 14$ ($R_s = 13$).

grid size	N	100	200	400	782
	E_N	-8.4888	-18.1712	-35.9625	-90.2027
8192^3	er_T	0.0010	0.0044	0.0074	0.0064
	$er_{T,rel}$	10^{-4}	$2 \cdot 10^{-4}$	$2 \cdot 10^{-4}$	10^{-4}
16384^3	er_T	0.0015	0.0010	0.002	0.0001
	$er_{T,rel}$	$2 \cdot 10^{-4}$	10^{-4}	10^{-4}	10^{-5}

TABLE 6

The accuracy of the tensor approximation $E_{N,T}$ to E_N of the interaction energy of an N-particle cluster when using the RS tensor approximation with $R_l = 12$ ($R_s = 13$), where $R_{RS,C}$ is the reduced canonical rank of the RS tensor representation.

N	512	1728	2048	4096
E_N	51.8439	-133.9060	-138.5562	-207.8477
er_T	0.1145	0.1317	0.2263	0.2174
$er_{T,rel}$	0.0022	0.001	0.0016	0.001
NR	12800	43200	51200	102400
$R_{RS,C}$	688	1248	1256	1740

Table 4 shows the accuracy of the tensor approximation $E_{N,T}$ to the interaction energy of an N-particle cluster E_N when using full canonical tensor representation of the cluster potential ($R_s = 0$). The absolute $er_T = E_N - E_{N,T}$ and relative $er_{T,rel} = (E_N - E_{N,T})/E_N$ errors are shown for N-particle systems of different sizes and are computed by tensor representation of the potentials on the $n \times n \times n$ 3D Cartesian grids with $n = 8192$ and $n = 16384$, with mesh sizes $6.8\,10^{-3}$ Å and $3.4\,10^{-3}$ Å, respectively. We use the data for a protein-type molecular system provided by the authors of [44]. This table indicates that the relative error of tensor-based computation of the interaction energy remains of the order of 10^{-4} for the considered range of grid sizes and particle numbers N. Table 5 presents the error of energy computation for the same clusters by (4.7) by using the RS tensor format with $R_l = 14$ and $R_s = 13$. Remarkably, the approximation error does not exceed the errors in Table 4.

Table 6 shows the results for several clusters of particles generated by random assignment of charges z_j to finite lattices of size 8^3, 12^3, $16 \times 16 \times 8$, and 16^3. The Newton kernel is approximated with $\varepsilon_N = 10^{-4}$ on the grid of size $n^3 = 4096^3$, with the rank $R = 25$. Computation of the interaction energy was performed by using only the long-range part with $R_l = 12$. For rank reduction the multigrid C2T algorithm is used [39], with the rank truncation parameters $\varepsilon_{C2T} = 10^{-5}$, $\varepsilon_{T2C} = 10^{-6}$. The box size is about $20 \times 20 \times 20$ Å, while the mesh size is $h = 0.005$ Å. Table 6 illustrates

that the relative accuracy of energy calculations made using the RS tensor format remains of the order of 10^{-3} almost independently of the cluster size.

5. Conclusions. In this paper, we have introduced and analyzed the new range-separated canonical and Tucker tensor formats for modeling long-range interaction potentials in multiparticle systems. One can distinguish the RS tensors from the conventional rank-structured representations due to their intrinsic features, originating from tensor approximation to multivariate functions with multiple singularities, in particular, generated by a weighted sum of the classical Green's kernels.

We have shown that the tensor approximation to the interaction potentials allows one to split their long- and short-range parts, providing efficient representation and numerical treatment of multiparticle systems in RS tensor formats. Indeed, the long-range part in the potential sum can be represented on a grid by the low-rank canonical/Tucker tensor globally in the computational box. In turn, its short-range component is parametrized by a reference tensor of local support and a list of particle coordinates and charges. In particular, we prove that the Tucker rank of the long-range part in the N-particle potential depends logarithmically on N. The model parameters specifying the short- and long-range splitting in the generating potential are chosen adaptively depending on the target accuracy and typical interparticle distances.

The RS formats prove to be well suited for summation of the electrostatic potentials in large many-particle systems in a box (e.g., proteins or large molecular clusters), providing a low-parametric tensor representation of the total potential at any point of the fine 3D $n \times n \times n$ Cartesian grid. For the computer realization of the RS tensor decomposition, a canonical-to-Tucker rank reduction algorithm is applied resulting in the $O(dn \log N)$ grid representation of the long-range part in the many-particle potential in $\mathbb{R}^d$. Notice that most existing approaches are limited by the $O(n^d)$ volume complexity, contrary to the almost linear scaling in the univariate mesh size n and dimension parameter d inherent to the RS tensor format. Numerical tests confirm the theoretical rank estimates and the asymptotically optimal complexity bound $O(N)$. In particular, the electrostatic potential for N-particle systems (up to several thousands of atoms) is computed in MATLAB with controllable accuracy, using large 3D representation grids of size up to $n^3 = 10^{12}$.

As examples of possible applications, we described the tensor-based calculation of the electrostatic interaction energy of protein-type systems. We observed that the application of the RS canonical/Tucker formats exhibits very mild limitations on the system size. The applications of RS tensors in multidimensional scattered data modeling are also discussed.

The presented analysis of the RS tensor format indicates its potential benefits in various applications related to the modeling of many-particle systems with quasiuniform distribution. It addresses a number of new interesting theoretical and algorithmic questions on the rank-structured tensor approximation of multivariate functions with generally located point singularities.

REFERENCES

[1] T. Beck, *Real-space mesh techniques in density-functional theory*, Rev. Mod. Phys., 72 (2000), pp. 1041–1080.

[2] P. Benner, S. Dolgov, V. Khoromskaia, and B. N. Khoromskij, *Fast iterative solution of the Bethe-Salpeter eigenvalue problem using low-rank and QTT tensor approximation*, J. Comput. Phys., 334 (2017), pp. 221–239.

[3] P. Benner, S. Dolgov, A. Onwunta, and M. Stoll, *Low-rank solvers for unsteady Stokes–Brinkman optimal control problem with random data*, Comput. Methods Appl. Mech. Engrg., 304 (2016), pp. 26–54.
[4] P. Benner, S. Gugercin, and K. Willcox, *A survey of projection-based model reduction methods for parametric dynamical systems*, SIAM Rev., 57 (2015), pp. 483–531.
[5] P. Benner, V. Khoromskaia, and B. N. Khoromskij, *Range-separated Tensor Formats for Numerical Modeling of Many-Particle Interaction Potentials*, preprint, arXiv:1606.09218v3, 2016.
[6] P. Benner, V. Khoromskaia, and B. N. Khoromskij, *A reduced basis approach for calculation of the Bethe–Salpeter excitation energies using low-rank tensor factorisations*, Mol. Phys., 114 (2016), pp. 1148–1161.
[7] P. Benner, V. L. Mehrmann, and D. C. Sorensen, *Dimension Reduction of Large-Scale Systems*, Lecture Notes in Computational Science and Engineering 45, Springer, Berlin, 2005.
[8] C. Bertoglio and B. N. Khoromskij, *Low-rank quadrature-based tensor approximation of the Galerkin projected Newton/Yukawa kernels*, Comput. Phys. Comm., 183 (2012), pp. 904–912.
[9] G. Beylkin, J. Garcke, and M. J. Mohlenkamp, *Multivariate regression and machine learning with sums of separable functions*, SIAM J. Sci. Comput., 31 (2009), pp. 1840–1857.
[10] S. F. Boys, G. B. Cook, C. M. Reeves, and I. Shavitt, *Automatic fundamental calculations of molecular structure*, Nature, 178 (1956), pp. 1207–1209.
[11] D. Braess, *Nonlinear Approximation Theory*, Springer, Berlin, 1986.
[12] M. D. Buhmann, *Radial Basis Functions*, Cambridge University Press, Cambridge, 2003.
[13] E. Cances, V. Ehrlacher, and T. Lelievre, *Greedy algorithms for high-dimensional eigenvalue problems*, Constr. Approx., 40 (2014), pp. 387–423.
[14] W. Dahmen, R. Devore, L. Grasedyck, and A. Süli, *Tensor-sparsity of solutions to high-dimensional elliptic partial differential equations*, Found. Comput. Math., 16 (2016), pp. 813–874.
[15] T. Darten, D. York, and L. Pedersen, *Particle mesh Ewald: An N·log (N) method for Ewald sums in large systems*, J. Chem. Phys., 98 (1993), pp. 10089–10091.
[16] L. De Lathauwer, B. De Moor, and J. Vandewalle, *A multilinear singular value decomposition*, SIAM J. Matrix Anal. Appl., 21 (2000), pp. 1253–1278.
[17] H. De Sterck, *An nonlinear GMRES optimization algorithm for canonical tensor decomposition*, SIAM J. Sci. Comput., 34 (2012), pp. A1351–A1379.
[18] H. De Sterck and K. Miller, *An adaptive algebraic multigrid algorithm for low-rank canonical tensor decomposition*, SIAM J. Sci. Comput., 35 (2013), pp. B1–B24.
[19] M. Deserno and C. Holm, *How to mesh up Ewald sums.* I. *A theoretical and numerical comparison of various particle mesh routines*, J. Chem. Phys., 109 (1998), pp. 7678–7693.
[20] M. Deserno and C. Holm, *How to mesh up Ewald sums.* II. *An accurate error estimate for the particle-particle-particle-mesh algorithm*, J. Chem. Phys., 109 (1998), pp. 7694–7701.
[21] S. V. Dolgov, B. N. Khoromskij, and I. V. Oseledets, *Fast solution of parabolic problems in the tensor train/quantized tensor train format with initial application to the Fokker–Planck equation*, SIAM J. Sci. Comput., 34 (2012), pp. A3016–A3038.
[22] P. Ewald, *Die Berechnung optischer und elektrostatischer Gitterpotentiale*, Ann. Phys., 369 (1921), pp. 253–287.
[23] B. Fornberg and N. Flyer, *A Primer on Radial Basis Functions with Applications to the Geosciences*, CBMS-NSF Regional Conference Series in Applied Mathematics 87, SIAM, Philadelphia, PA, 2015.
[24] L. Grasedyck, D. Kressner, and C. Tobler, *A literature survey of low-rank tensor approximation techniques*, GAMM-Mitt., 36 (2013), pp. 53-78.
[25] L. Greengard and V. Rochlin, *A fast algorithm for particle simulations*, J. Comput. Phys., 73 (1987), pp. 325–348.
[26] W. Hackbusch and B. Khoromskij, *Low-rank Kronecker-product approximation to multi-dimensional nonlocal operators. Part* I. *Separable approximation of multi-variate functions*, Computing, 76 (2006), pp. 177–202.
[27] W. Hackbusch and R. Schneider, *Tensor spaces and hierarchical tensor representations*, in Extraction of Quantifiable Information for Complex Systems, Lecture Notes in Computational Science and Engineering 102, S. Dahlke et al., eds., Springer, Cham, 2014, pp. 237–262.
[28] J. S. Hesthaven, G. Rozza, and B. Stamm, *Certified Reduced Basis Methods for Parametrized Partial Differential Equations*, Springer, Berlin, 2016.
[29] R. W. Hockney and J. W. Eastwood, *Computer Simulation Using Particles*, IOP Publishing, Bristol, 1988.

[30] P. H. Hünenberger and J. A. McCammon, *Effect of artificial periodicity in simulations of biomolecules under Ewald boundary conditions: A continuum electrostatics study*, Biophys. Chem., 78 (1999), pp. 69–88.
[31] A. Iske, *Multiresolution Methods in Scattered Data Modelling*, Springer, Berlin, 2004.
[32] V. Khoromskaia and B. N. Khoromskij, *Grid-based lattice summation of electrostatic potentials by assembled rank-structured tensor approximation*, Comput. Phys. Comm., 185 (2014), pp. 3162–3174.
[33] V. Khoromskaia and B. N. Khoromskij, *Tensor numerical methods in quantum chemistry: From Hartree–Fock to excitation energies*, Phys. Chem. Chem. Phys., 17 (2015), pp. 31491–31509.
[34] V. Khoromskaia and B. N. Khoromskij, *Fast tensor method for summation of long-range potentials on 3D lattices with defects*, Numer. Linear Algebra Appl., 23 (2016), pp. 249–271.
[35] B. N. Khoromskij, *Structured rank-$(r_1, \dots, r_d)$ decomposition of function-related operators in $\mathbb{R}^d$*, Comput. Methods Appl. Math., 6 (2006), pp. 194–220.
[36] B. N. Khoromskij, *$O(d \log N)$-quantics approximation of N-d tensors in high-dimensional numerical modeling*, Constr. Approx., 34 (2011), pp. 257–289.
[37] B. N. Khoromskij, *Tensors-structured numerical methods in scientific computing: Survey on recent advances*, Chemometr. Intell. Lab. Syst., 110 (2012), pp. 1–19.
[38] B. N. Khoromskij and V. Khoromskaia, *Low rank Tucker tensor approximation to the classical potentials*, Cent. Eur. J. Math., 5 (2007), pp. 523–550.
[39] B. N. Khoromskij and V. Khoromskaia, *Multigrid accelerated tensor approximation of function related multidimensional arrays*, SIAM J. Sci. Comput., 31 (2009), pp. 3002–3026.
[40] T. G. Kolda, *Orthogonal tensor decompositions*, SIAM J. Matrix Anal. Appl., 23 (2001), pp. 243–255.
[41] T. G. Kolda and B. W. Bader, *Tensor decompositions and applications*, SIAM Rev., 51 (2009), pp. 455–500.
[42] D. Kressner, M. Steinlechner, and A. Uschmajew, *Low-rank tensor methods with subspace correction for symmetric eigenvalue problems*, SIAM J. Sci. Comput., 36 (2014), pp. A2346 –A2368.
[43] K. N. Kudin and G. E. Scuseria, *Revisiting infinite lattice sums with the periodic fast multipole method*, J. Chem. Phys., 121 (2004), pp. 2886–2890.
[44] C. Kweyu, M. Hess, L. Feng, M. Stein, and P. Benner, *Reduced basis method for Poisson-Boltzmann equation*, in Proceedings of the 7th European Congress on Computational Methods in Applied Sciences and Engineering, Athens, 2016, pp. 4187–4195.
[45] D. Lindbo and A.-K. Tornberg, *Fast and spectrally accurate Ewald summation for 2-periodic electrostatic systems*, J. Chem. Phys., 136 (2012), 164111.
[46] F. Lipparini, B. Stamm, E. Cances, Y. Maday, and B. Mennucci, *Fast domain decomposition algorithm for continuum solvation models: Energy and first derivatives*, J. Chem. Theory Comput., 9 (2013), pp. 3637–3648.
[47] H. G. Matthies, A. Litvinenko, O. Pajonk, B. V. Rosic, and E. Zander, *Parametric and uncertainty computations with tensor product representations*, in Uncertainty Quantification in Scientific Computing, M. Dienstfrey and R. F. Boisvert, eds., Springer, Berlin, 2012, pp. 139–150.
[48] I. V. Oseledets, *Approximation of $2^d \times 2^d$ matrices using tensor decomposition*, SIAM J. Matrix Anal. Appl., 31 (2010), pp. 2130–2145.
[49] I. V. Oseledets, *Tensor-train decomposition*, SIAM J. Sci. Comput., 33 (2011), pp. 2295–2317.
[50] E. L. Pollock and J. Glosli, *Comments on $P(3)m$, FMM and the Ewald method for large periodic Coulombic systems*, Comput. Phys. Comm., 95 (1996), pp. 93–110.
[51] A. Quarteroni, A. Manzoni, and F. Negri, *Reduced Basis Methods for Partial Differential Equations: An Introduction*, Springer, Cham, 2016.
[52] M. Rakhuba and I. Oseledets, *Grid-based Electronic Structure Calculations: The Tensor Decomposition Approach*, preprint, arXiv:1508.07632, 2015.
[53] M. Stein, R. R. Gabdoulline, and R. C. Wade, *Cross-species analysis of the glycolytic pathway by comparison of molecular interaction fields*, Mol. Biosyst., 6 (2010), pp. 162–174.
[54] F. Stenger, *Numerical Methods Based on Sinc and Analytic Functions*, Springer, New York, 1993.
[55] J. Toulouse, F. Colonna, and A. Savin, *Long-range–short-range separation of the electron-electron interaction in density-functional theory*, Phys. Rev. A, 70 (2004), 062505.
[56] M. Zuzovski, A. Boag, and A. Natan, *An auxiliary grid method for the calculation of electrostatic terms in density functional theory on a real-space grid*, Phys. Chem. Chem. Phys., 17 (2015), pp. 31550–31557.